indicated perlecan's 369-kDa core protein consisted of five distinct domains: domain I is a unique N-terminal sequence that was later shown to contain the sites for heparan sulfate attachment [4]; domain II is similar to the cholesterol binding region of the low density lipoprotein (LDL) receptor; domain III is similar to the short arm of the laminin A chain; domain IV is the largest domain and contains 14 repeats of IgG-like motifs similar to those in neural cell adhesion molecule (N-CAM); and domain V is similar to G subdomains of the laminin chain interrupted by EGF-like motifs. Perlecan's name is derived from its rotary shadowed image in the electron microscope as a string of pearls [16–19]. Perlecan is expressed in multiple forms. The structure of human perlecan is essentially identical to murine perlecan except that domain IV contains 21 repeats of the IgG-like motifs, which increases the core protein to 466 kDa [20]. This longer form of perlecan was shown to be expressed in mice as an alternatively spliced form [21]. A homologue of perlecan is also present in the basement membranes of *C. elegans* [22,23] and *Drosophila* [24]. Mutations in the alternatively spliced perlecan gene in *C. elegans* produce defective muscle development and cause paralysis [22,23]. Perlecan may contain only heparan sulfate chains [12] or both heparan and chondroitin sulfate chains [25]. The size of the GAG chains also varies according to tissue and cell type.

In addition to its presence in all basement membranes, perlecan is also present in the extracellular matrix of the growth plate and in articular cartilage, where it contains both heparan sulfate and chondroitin sulfate chains [25,26]. Interestingly, the greatest deposition of perlecan during embryonic development was found to be in cartilage undergoing endochondral ossification in the growth plate during long bone development [27]. Especially strong expression of perlecan is observed in the prehypertrophic and hypertrophic zones [28]. Although perlecan is considered a "matrix proteoglycan," immunostaining of cartilage sections with antisera to perlecan showed that it is localized at the pericellular space of chondrocytes and in the matrix between chondrocytes [26,28].

The human gene for perlecan (*HSPG2*) is larger than 120 kb in size. The gene structure was analyzed, and the number of exons was determined to be 94 [29]. However, the recent human chromosome 1 working draft sequence revealed that the perlecan gene consists of 97 exons (GenBank accession number NT_004576) [30,31]. The exon-intron organization shows a good correlation with the corresponding domains of the homologous genes. This suggests that the perlecan gene evolved by exon shuffling and gene duplication of a common ancestor. The promoter of the perlecan gene lacks TATA or CATT boxes, which are characteristic for house-keeping genes. Some regulatory regions have been identified, e.g., transforming growth factor-β (TGF-β) responsiveness [32].

Molecular interactions

Perlecan binds a number of extracellular matrix molecules, cell surface receptors, and growth factors, suggesting that perlecan acts as a glue to stabilize matrix organization and cell-matrix interaction and to modulate growth factor signaling for cell proliferation and differentiation [33,34]. Perlecan has been shown to bind basement membrane proteins including laminin, collagen IV, and nidogen/entactin [35]. It also binds other extracellular matrix including fibulin and fibronectin. Binding domains of perlecan for these interactions have been identified using recombinant proteins. Domain V interacts with cell surface receptors such as integrin $\beta 1$ and α-dystroglycan [36,37]. Many growth factors such as fibroblast growth factor (FGF) and platelet-derived growth factor (PDGF) bind the heparan sulfate chains and the protein core of perlecan [38–40]. It has been shown that perlecan is a low-affinity binding molecule for β-FGF and promotes mitogenesis and angiogenesis [41].

Gene knockout mice

Gene knockouts in mice have been useful in identifying the essential role of genes in development and tissue organization. The perlecan-null mutation in mice was independently accomplished by two research groups [28,42] and they reported similar perinatal lethal chondrodysplasia. Some of the *perlecan* $-/-$ mice died at embryonic day 10.5 with defective cephalic and cardiac development. Electron microscopy indicates that this may be due to altered basement membrane formation in the absence of perlecan. The remaining *perlecan* $-/-$ mice go on to develop skeletal dysplasia characterized by shortened long bones and craniofacial abnormalities and then die shortly after birth. Histological evaluation of the *perlecan* $-/-$ mice revealed a disorganized growth plate with reduced chondrocyte proliferation and differentiation and defective endochondral ossification [28,42]. Severe disruption of the matrix structure in the hypertrophic zone was observed especially late stages of development. Initially, no significant cartilage abnormalities were found prior to embryonic day 13.5, at which time endochondral ossification starts and thereafter disruption of the matrix became obvious and progressively severe. This accounted for the shortened long bones. Interestingly, abnormalities of phalange cartilage were less severe. Thus, perlecan is essential for normal cartilage development in mice.

The obligatory role that perlecan plays in cartilage development is not known. Perlecan isolated from non-cartilage cells and tissues has been shown to bind FGFs and growth factor-binding proteins by interactions with perlecan's core protein and its GAG chains [43–47]. FGFs are a family of proteins that act as intercellular signals in a wide variety of developmental processes [48], including limb development [49]. Transgenic mice over-expressing FGF-2 [50] and FGF-9 [51] exhibit defective growth plate development. More recently, it was shown using gene knockout mice that FGF-18 plays a critical role in endochondral ossification by increasing chondrocyte proliferation and differentiation and Indian hedgehog (Ihh) signaling [52]. The growth plate phenotype of the *Fgf18* knockout mice is similar to *Fgfr3* knockout mice, which are characterized by extended growth plates due to increased proliferating and

hypertrophic chondrocyte zones. Opposite cartilage abnormalities, i.e., short growth plate due to reduced proliferation and differentiation of chondrocytes, were observed in the most common human lethal chondrodysplasia, thanatophoric dysplasia type I, which is caused by activating mutations in *Fgfr3* [53]. FGF-R3c is a chondrocyte-specific receptor that suppresses expression of Ihh, which promotes chondrocyte proliferation. Ihh [54] has been shown to bind to heparin, a structural homologue of heparan sulfate, and to contain an attached cholesterol moiety [55,56]. While perlecan has not yet been demonstrated to bind to Ihh, perlecan does have heparan sulfate chains attached to its domain I [4], and domain II of its core protein has structural similarity to the region of the LDL receptor that binds cholesterol. Thus, perlecan could bind to both the cholesterol moiety and the heparan binding site of Ihh and thereby provide a very specific interaction. We and others have proposed [28,57] that perlecan could be a participant in the signaling pathways that regulate chondrocyte proliferation and hypertrophy. The heparan sulfate chains on perlecan may modulate the activity of an FGF receptor (FGF-R3) in growth plate chondrocytes by binding FGF [58]. Alternatively, or additionally, perlecan may modulate parathyroid hormone related peptide expression by regulating the diffusion of Ihh in the growth plate [59]. Another function of perlecan in cartilage development could be to stabilize matrix and cell-matrix interactions. Without perlecan, the matrix structure of chondrocytes is disrupted, and without a stable matrix cells are not able to differentiate.

Dyssegmental dysplasia, Silverman-Handmaker type

Similarities of the skeletal abnormalities of perlecan knockout mice led to identification of a human disorder, Dyssegmental dysplasia, Silverman-Handmaker type. This is a rare lethal autosomal recessive skeletal dysplasia characterized by anysospondyly and micromelia. Three patients were identified for perlecan mutations. A homozygous 89-bp duplication mutation was found in exon 36 of the perlecan gene in a pair of siblings with this dysplasia [60]. Heterozygous point mutations were identified at the donor site of exon 54 and at the middle of exon 73 in a third unrelated patient, causing exon skipping. These mutations are predicted to produce premature termination codons. Immunostaining and Western blotting revealed that truncated proteins were synthesized but not secreted. Thus, this dysplasia is caused by functional null mutations of the perlecan gene similar to the gene knockout mice [61].

Neuromuscular junction of knockout mice

Perlecan is present in muscle basement membranes and is enriched at the neuromuscular junction [62,63]. This junction forms a highly specialized structure where a unique set of molecules such as acetylcholinesterase, acetylcholine receptors, agrin, dystroglycans, rapsyn, and utrophin are clustered. In skeletal muscles, acetylcholine acts as a neurotransmitter. It binds the acetylcholine receptor on the muscle cell surface, activates Na channels, and induces muscle contraction. The esterase rapidly inactivates this process for muscle relaxation and recycling of acetylcholine. The collagen-tail form of the acetylcholine esterase is preferentially expressed in innervated regions of muscles and is shown to bind perlecan *in vitro* [64]. In the perlecan knockout mice, muscle development and differentiation appear to be normal and the nerve terminals are normally formed. Clustering molecules are present at the neuromuscular junction of the mutant mouse muscles. However, the acetylcholine esterase is completely absent at the neuromuscular junctions, although it is synthesized normally [65]. Thus, perlecan is essential for localizing acetylcholine esterase at the neuromuscular junction.

Schwartz-Jampel syndrome

Schwartz-Jampel syndrome was initially identified for perlecan mutations by positional cloning and gene linkage [30]. This syndrome is characterized by a unique combination of myotonia and chondrodysplasia, and unlike patients with the dyssegmental dysplasia, patients with Schwartz-Jampel syndrome survive. Characterization of the perlecan gene in these patients showed that it contained homozygous missense and splicing mutations that could result in either truncated perlecan missing part of domain IV and the whole domain V or molecules defective in disulfide bonds in domain III. Recent studies on additional Schwartz-Jampel syndrome patients [31] revealed various types of mutations that resulted in various forms of perlecan. For example, heterozygous mutations produce either truncated perlecan that lacks domain V or significantly reduced levels of wild-type perlecan. A homozygous 7-kb deletion resulted in reduced amounts of nearly full-length perlecan. Unlike the dyssegmental dysplasia syndrome, the Schwartz-Jampel syndrome mutations result in different forms of perlecan in reduced levels that are secreted to the extracellular matrix and are partially functional. These findings indicate an important role of perlecan in neuromuscular function and cartilage formation. Recently, Spanger et al. [66] reported that clinical examinations indicated that other skeletal dysplasias previously identified as chondrodysplasia, (kyphomelic chondrodysplasia, micromelic chondrodysplasia, and Burton disease), could be reclassified. Thus, Schwartz-Jampel phenotype encompasses a wide spectrum.

References

1 Roden L, Koerner T, Olson C, Schwartz NB, Mechanisms of chain initiation in the biosynthesis of connective tissue polysaccharides, *Fed Proc* **44**, 373–80 (1985).
2 Bourdon MA, Krusius T, Campbell S, Schwartz NB, Ruoslahti E, Identification and synthesis of a recognition signal for the attachment of glycosaminoglycans to proteins, *Proc Natl Acad Sci* **84**, 3194–8 (1987).
3 Kitagawa H, Shimakawa H, Sugahara K, The tumor suppressor EXT-like gene EXTL2 encodes an alpha1, 4-N-acetylhexosaminyltrasferase that transfers N-acetylgalactosamine and

N-acetylglucosamine to the common glycosaminoglycan-protein linkage region. The key enzyme for the chain initiation of heparan sulfate, *J Biol Chem* **274**, 13933–7 (1999).
4 Dolan M, Horchar T, Rigatti B, Hassell JR, Identification of sites in domain I of perlecan that regulate heparan sulfate synthesis, *J Biol Chem* **272**(7), 4316–22 (1997).
5 Zhang L, Esko JD, Amino acid determinants that drive heparan sulfate assembly in a proteoglycan, *J Bio Chem* **269**, 19295–9 (1994).
6 Zhang L, David G, Esko JD, Repetitive Ser-Gly sequences enhance heparan sulfate assembly in proteoglycans, *J Biol Chem* **270**, 27127–35 (1995).
7 McCormick C, Leduc Y, Martindale D, Mattison K, Esford LE, Dyer AP, Tufaro F, The putative tumour suppressor EXT1 alters the expression of cell-surface heparan sulfate, *Nat Genet* **19**, 158–61 (1998).
8 Lind T, Tufaro F, McCormick C, Lindahl U, Lidholt K, The putative tumor suppressors EXT1 and EXT2 are glycosyltransferases required for the biosynthesis of heparan sulfate, *J Biol Chem* **273**, 26265–8 (1998).
9 Bernfield M, Götte M, Park PW, Reizes O, Fitzgerald ML, Lincecum J, Zako M, Functions of cell surface heparan sulfate proteoglycans, *Annu Rev Biochem* **68**, 729–77 (1999).
10 Dunlevy JR, Hassell JR, Heparan sulfate proteoglycans in basement membranes. In *Proteoglycans: Structure, Biology and Molecular Interactions*, edited by Iozzo RV (Marcel Dekker, Inc., New York), 2000.
11 Knudson CB, Knudson W, Cartilage proteoglycans, *Semin Cell Dev Biol* **12**, 69–78 (2001).
12 Hassell JR, Robey PG, Barrach HJ, Wilczek J, Rennard SI, Martin GR, Isolation of a heparan sulfate-containing proteoglycan from basement membrane, *Proc Natl Acad Sci* **77**(8), 4494–8 (1980).
13 Ledbetter SR, Tyree B, Hassell JR, Horigan EA, Identification of the precursor protein to basement membrane heparan sulfate proteoglycans, *J Biol Chem* **260**(13), 8106–13 (1985).
14 Ledbetter SR, Fisher LW, Hassell JR, Domain structure of the basement membrane heparan sulfate proteoglycan, *Biochem* **26**(4), 988–95 (1987).
15 Noonan DM, Horigan E, Ledbetter S, Vogeli G, Sasaki M, Yamada Y, Hassell JR, Identification of cDNA clones encoding different domains of the basement membrane heparan sulfate proteoglycan, *J Biol Chem* **263**(31), 16379–87 (1998).
16 Noonan DM, Fulle A, Valente P, Cai S, Horigan E, Sasaki M, Yamada Y, Hassell JR, The complete sequence of perlecan, a basement membrane heparan sulfate proteoglycan, reveals extensive similarity with laminin A chain, low density lipoprotein-receptor, and the neural cell adhesion molecule, *J Biol Chem* **266**(34), 22939–47 (1991).
17 Paulsson M, Yurchenco PD, Ruben GC, Engel J, Timpl R, Structure of low density heparan sulfate proteoglycan isolated from a mouse tumor basement membrane, *J Mol Biol* **197**, 297–313 (1987).
18 Yurchenco PD, Cheng YS, Ruben GC, Self-assembly of a high molecular weight basement membrane heparan sulfate proteoglycan into dimers and oligomers, *J Biol Chem* **262**, 17668–76 (1987).
19 Laurie GW, Inoue S, Bing JT, Hassell JR, Visualization of the large heparan sulfate proteoglycan from basement membranes, *Am J Anat* **181**, 320–6 (1988).
20 Murdoch AD, Dodge GR, Cohen I, Tuan RS, Iozzo RV, Primary structure of the human heparan sulfate proteoglycan from basement membrane (HSPG2/perlecan). A chimeric molecule with multiple domains homologous to the low density lipoprotein receptor, laminin, neural cell adhesion molecules, and epidermal growth factor, *J Biol Chem* **267**(12), 8544–57 (1992).
21 Noonan DM, Hassell JR, Perlecan, the large low density proteoglycan of basement membranes: Structure and variant forms, *Kidney International* **43**(1), 53–60 (1993).
22 Rogalski TM, Williams BD, Mullen GP, Moerman DG, Products of the unc-52 gene in Caenorhabditis elegans are homologous to the core protein of the mammalian basement membrane heparan sulfate proteoglycan, *Genes Dev* **7**, 1471–84 (1993).
23 Friedrich MV, Schneider M, Timpl R, Baumgartner S, Perlecan domain V of Drosophila melanogaster. Sequence, recombinant analysis and tissue expression, *Eur J Biochem* **267**, 3149–59 (2000).
24 Rogalski TM, Mullen GP, Bush JA, Gilchrist EJ, Moerman DG, UNC-52/perlecan isoform diversity and function in Caenorhabditis elegans, *Biochem Soc Trans* **29**, 171–6 (2001).
25 Govindraj P, West L, Koob TJ, Neame P, Doege K, Hassell J, Isolation and identification of the major heparan sulfate proteoglycans in the developing bovine rib growth plate, *J Bio Chem* **277**, 19461–9 (2002).
26 SundarRaj N, Fite D, Ledbetter S, Chakravarti S, Hassell JR, Perlecan is a component of cartilage matrix and promotes chondrocyte attachment, *J Cell Sci* **108**(Pt 7), 2663–72 (1995).
27 Handler M, Yurchenco PD, Iozzo RV, Developmental expression of perlecan during murine embryogenesis, *Dev Dyn* **210**(2), 130–45 (1997).
28 Arikawa-Hirasawa E, Watanabe H, Takami H, Hassell JR, Yamada Y, Perlecan is essential for cartilage and cephalic development, *Nat Genet* **23**, 354–8 (1999).
29 Cohen IR, Grassel S, Murdoch AD, Iozzo RV, Structural characterization of the complete human perlecan gene and its promoter, *Proc Natl Acad Sci USA* **90**, 10404–8.
30 Nicole S, Davoine CS, Topaloglu H, Cattolico L, Barral D, Beighton P, Hamida CB, Hammouda H, Cruaud C, White PS, Samson D, Urtizberea JA, Lehmann-Horn F, Weissenbach J, Hentati F, Fontaine B, Perlecan, the major proteoglycan of basement membranes, is altered in patients with Schwartz-Jampel syndrome (chondrodystrophic myotonia), *Nat Genet* **26**, 480–3 (2000).
31 Arikawa-Hirasawa E, Le AH, Nishino I, Nonaka I, Ho NC, Francomano CA, Govindraj P, Hassell JR, Devaney JM, Spranger J, Stevenson RE, Iannaccone S, Dalakas MC, Yamada Y, Structural and functional mutations of the perlecan gene cause Schwartz-Jampel syndrome, with myotonic myopathy and chondrodysplasia, *Am J Hum Genet* **70**, 1368–75 (2002).
32 Iozzo RV, Pillarisetti J, Sharma B, Murdoch AD, Danielson KG, Uitto J, Mauviel A, Structural and functional characterization of the human perlecan gene promoter. Transcriptional activation by transforming growth factor-beta via a nuclear factor 1-binding element, *J Biol Chem* **272**, 5219–28 (1997).
33 Iozzo RV, Cohen IR, Grassel S, Murdoch AD, The biology of perlecan: The multifaceted heparan sulphate proteoglycan of basement membranes and pericellular matrices, *Biochem J* **302**, 625–39 (1994).
34 Timpl R, Brown JC, Supramolecular assembly of basement membranes, *Bioessays* **18**, 123–32 (1996).
35 Hopf M, Gohring W, Kohfeldt E, Yamada Y, Timpl R, Recombinant domain IV of perlecan binds to nidogens, laminin-nidogen

complex, fibronectin, fibulin-2 and heparin, *Eur J Biochem* **259**, 917–25 (1999).
36 Brown JC, Sasaki T, Gohring W, Yamada Y, Timpl R, The C-terminal domain V of perlecan promotes beta1 integrin-mediated cell adhesion, binds heparin, nidogen and fibulin-2 and can be modified by glycosaminoglycans, *Eur J Biochem* **250**, 39–46 (1997).
37 Talts JF, Andac Z, Gohring W, Brancaccio A, Timpl R, Binding of the G domains of laminin alpha1 and alpha2 chains and perlecan to heparin, sulfatides, alpha-dystroglycan and several extracellular matrix proteins, *Embo J* **18**, 863–70 (1999).
38 Gohring W, Sasaki T, Heldin CH, Timpl R, Mapping of the binding of platelet-derived growth factor to distinct domains of the basement membrane proteins BM-40 and perlecan and distinction from the BM-40 collagen-binding epitope, *Eur J Biochem* **255**, 60–6 (1998).
39 Mongiat M, Taylor K, Otto J, Aho S, Uitto J, Whitelock JM, Iozzo RV, The protein core of the proteoglycan perlecan binds specifically to fibroblast growth factor-7, *J Biol Chem* **275**, 7095–100 (2000).
40 Whitelock JM, Murdoch AD, Iozzo RV, Underwood PA, The degradation of human endothelial cell-derived perlecan and release of bound basic fibroblast growth factor by stromelysin, collagenase, plasmin, and heparanases, *J Biol Chem* **271**, 10079–86 (1996).
41 Aviezer D, Hecht D, Safran M, Eisinger M, David G, Yayon A, Perlecan, basal lamina proteoglycan, promotes basic fibroblast growth factor-receptor binding, mitogenesis, and angiogenesis, *Cell* **79**, 1005–13 (1994).
42 Costell M, Gustafsson E, Aszodi A, Morgelin M, Bloch W, Hunziker E, Addicks K, Timpl R, Fassler R, Perlecan maintains the integrity of cartilage and some basement membranes, *J Cell Biol* **147**(5), 1109–22 (1999).
43 Aviezer A, Hecht D, Safran M, Eisinger M, David G, Yayon A, Perlecan, basal lamina proteoglycan, promotes basic fibroblast growth factor-receptor binding, mitogenesis, and angiogenesis, *Cell* **79**, 1005–13 (1994).
44 Forsten KE, Courant NA, Nugent MA, Endothelial proteoglycans inhibit bFGF binding and mitogenesis, *J Cell Physiol* **172**, 209–20 (1997).
45 Larrain J, Alvarez J, Hassell JR, Brandan E, Expression of perlecan, a proteoglycan that binds myogenic inhibitory basic fibroblast growth factor, is down regulated during skeletal muscle differentiation, *Exp Cell Res* **234**, 405–12 (1997).
46 Mongiat M, Otto J, Oldershaw R, Ferrer F, Sato JD, Iozzo RV, Fibroblast growth factor-binding protein is a novel partner for perlecan protein core, *J Biol Chem* **276**, 10263–71 (2001).
47 Knox S, Merry C, Stringer S, Melrose J, Whitelock J, Not all perlecans are equal: Interactions with fibroblast growth factor 2 (FGF-2) and FGF receptors, *J Biol Chem* **277**, 14657–65 (2002).
48 Yamaguchi TP, Rossant J, Fibroblast growth factors in mammalian development, *Curr Opin Genet Dev* **5**, 485–91 (1995).
49 Martin GR, The roles of FGFs in the early development of vertebrate limbs, *Genes Dev* **12**, 1571–86 (1998).
50 Coffin JD, Florkiewicz RZ, Neumann J, Mort-Hopkins T, Dorn GW 2nd, Lightfoot P, German R, Howles PN, Kier A, O'Toole BA et al., Abnormal bone growth and selective translational regulation in basic fibroblast growth factor (FGF-2) transgenic mice, *Mol Biol Cell* **6**, 1861–73 (1995).
51 Garofalo S, Kliger-Spatz M, Cooke JL, Wolstin O, Lumstrum GP, Moshkovitz SM, Horton WA, Yayon A, Skeletal dysplasia and defective chondrocyte differentiation by targeted overexpression of fibroblast growth factor 9 in transgenic mice, *J Bone Miner Res* **14**, 1909–15 (1999).
52 Liu Z, Xu J, Colvin JS, Ornitz DM, Coordination of chondrogenesis and osteogenesis by fibroblast growth factor 18, *Genes Dev* **16**, 859–69 (2002).
53 Tavormina PL, Shiang R, Thompson LM, Zhu YZ, Wilkin DJ, Lachman RS, Wilcox WR, Rimoin DL, Cohn DH, Wasmuth JJ, Thanatophoric dysplasia (types I and II) caused by distinct mutations in fibroblast growth factor receptor 3, *Nat Genet* **9**, 321–8 (1995).
54 St-Jacques B, Hammerschmidt M, McMahon AP, Indian hedgehog signaling regulates proliferation and differentiation of chondrocytes and is essential for bone formation, *Genes Dev* **13**, 2617 (1999).
55 Ingham PW, Hedgehog signaling: A tale of two lipids, *Science* **294**, 1879 (2001).
56 Lewis PM, Dunn MP, McMahon JA, Logan M, Martin JF, St-Jacques B, McMahon AP, Cholesterol modification of sonic hedgehog is required for long-range signaling activity and effective modulation of signaling by Ptc1, *Cell* **105**, 599–612 (2001).
57 Olsen BR, Life without perlecan has its problem, *J Cell Biol* **147**(5), 909–12 (1999).
58 Deng C, Wynshaw-Boris A, Zhou F, Kuo A, Leder P, Fibroblast growth factor receptor 3 is a negative regulator of bone growth, *Cell* **84**(6), 911–21 (1996).
59 Vortkamp A, Lee K, Lanske B, Segre GV, Kronenberg HM, Tabin CJ, Regulation of rate of cartilage differentiation by Indian hedgehog and PTH-related protein, *Science* **273**(5275), 613–22 (1996).
60 Arikawa-Hirasawa E, Wilcox WR, Le AH, Silverman N, Govindraj P, Hassell JR, Yamada Y, Dyssegmental dysplasia, Silverman-Handmaker type, is caused by functional null mutations of the perlecan gene, *Nat Genet* **27**, 431–4 (2001).
61 Arikawa-Hirasawa E, Wilcox WR, Yamada Y, Dyssegmental dysplasia, Silverman-Handmaker type: Unexpected role of perlecan in cartilage development, *Am J Med Genet* **106**, 254–7 (2001).
62 Bayne EK, Anderson MJ, Fambrough DM, Extracellular matrix organization in developing muscle: Correlation with acetylcholine receptor aggregates, *J Cell Biol* **99**, 1486–501 (1984).
63 Sanes JR, Schachner M, Covault J, Expression of several adhesive macromolecules (N-CAM, L1, J1, NILE, uvomorulin, laminin, fibronectin, and a heparan sulfate proteoglycan) in embryonic, adult, and denervated adult skeletal muscle, *J Cell Biol* **102**, 420–31 (1986).
64 Peng HB, Xie H, Rossi SG, Rotundo RL, Acetylcholinesterase clustering at the neuromuscular junction involves perlecan and dystroglycan, *J Cell Biol* **145**, 911–21 (1999).
65 Arikawa-Hirasawa E, Rossi SG, Rotundo RL, Yamada Y, Absence of acetylcholinesterase at the neuromuscular junctions of perlecan-null mice, *Nat Neurosci* **5**, 119–23 (2002).
66 Spranger J, Hall BD, Hane B, Srivastava A, Stevenson RE, Spectrum of Schwartz-Jampel syndrome includes micromelic chondrodysplasia, kyphomelic dysplasia, and Burton disease, *Am J Med Genet* **94**, 287–95 (2000).

DOI: 10.1093/brain/awg010 *Brain* (2003), **126**, 32–42

Haploinsufficiency at the α-synuclein gene underlies phenotypic severity in familial Parkinson's disease

Hirokazu Kobayashi,[1] Rejko Krüger,[3] Katerina Markopoulou,[5] Zbigniew Wszolek,[7] Bruce Chase,[6] Hikaru Taka,[2] Reiko Mineki,[2] Kimie Murayama,[2] Olaf Riess,[4] Yoshikuni Mizuno[1] and Nobutaka Hattori[1]

[1]*Department of Neurology and* [2]*Division of Biochemical Analysis, Juntendo University School of Medicine, Tokyo, Japan, Departments of* [3]*Neurology and* [4]*Medical Genetics, University of Tübingen, Tübingen, Germany,* [5]*Department of Neurological Sciences, University of Nebraska Medical Center and* [6]*Department of Biology, University of Nebraska at Omaha, Omaha, and* [7]*Department of Neurology, Mayo Clinic Jacksonville, USA*

Correspondence to: Nobutaka Hattori, MD, Department of Neurology Juntendo University School of Medicine, 2-1-1 Hongo, Bunkyo, Tokyo 113-8421, Japan
E-mail: nhattori@med.juntendo.ac.jp

Summary

To date, two point mutations, G209A and G88C, have been reported in the coding region of the α-synuclein gene in autosomal dominant familial Parkinson's disease. When translated, these lead to the missense mutations Ala53Thr and Ala30Pro, respectively. Reduced mRNA expression of the G209A allele was reported recently in a Greek–American family. Here, we show that α-synuclein mRNA is normally expressed in blood cells and report the results of an analysis of α-synuclein mRNA and protein expression in lymphoblastoid cell lines established from kindreds with the G209A and G88C mutations. mRNA expression was characterized using a TaqMan real-time quantitative reverse transcriptase–polymerase chain reaction (RT–PCR) assay. We assessed five affected and three unaffected members of a German family with the G88C mutation and two affected members in different, unrelated Greek families with the G209A mutation. The ratio of wild-type to mutant α-synuclein allele expression ranged from 2.2 to 9.2 in the affected individuals with a severe clinical phenotype. The ratios of the expression levels of the wild-type to mutant alleles were only slightly decreased in mild cases and were less than 1.0 in two asymptomatic heterozygotes. Sequence analysis of the RT–PCR products showed only the presence of G in position 88 and G in position 209 in severely affected heterozygotes of the German and Greek families, respectively. High performance liquid chromatography/mass spectrometry demonstrated that, relative to wild-type α-synuclein, there is a reduction of Ala30Pro α-synuclein in lymphoblastoid cell lines originating from severely affected, but not mildly affected G88C/+ heterozygotes. Taken together, these data indicate that there is haploinsufficiency at the α-synuclein gene and that the ratio of expression of the wild-type to mutant alleles correlates with the severity of the clinical phenotype. Furthermore, these findings suggest that haploinsufficiency of α-synuclein mutations may contribute to disease progression in these forms of familial Parkinson's disease.

Keywords: α-synuclein; haploinsufficiency; familial Parkinson's disease; G88C and G209A mutations

Abbreviations: ADFPD = autosomal dominant familial Parkinson's disease; GAPDH = glyceraldehyde-3-phosphate dehydrogenase; HPLC/MS = high performance liquid chromatography/mass spectrometry; RT–PCR = reverse transcriptase–polymerase chain reaction; RFLP = restriction fragment length polymorphism; SDS–PAGE = sodium dodecyl sulphate-polyacrylamide gel electrophoresis

Introduction

Parkinson's disease is the second most common neurodegenerative disorder in the ageing population. Although most patients with Parkinson's disease are sporadic cases, it is now clear that genetic factors contribute to the pathogenesis of Parkinson's disease (Polymeropoulos *et al.*, 1996, 1997; Gasser *et al.*, 1998; Kitada *et al.*, 1998). The discovery of two point mutations in the coding region of the α-synuclein gene in autosomal dominant familial Parkinson's disease (ADFPD) prompted a series of studies into the role of α-synuclein in both familial and sporadic Parkinson's disease (Polymeropoulos *et al.*, 1997; Spillantini *et al.*, 1997, 1998; Krüger *et al.*, 1998). The first mutation—a G-to-A transition in exon 4 that, if translated, results in an Ala53Pro missense mutation in α-synuclein—was identified in a large Italian–American multigenerational family with an ADFPD known as the Contursi kindred (Polymeropoulos *et al.*, 1996, 1997). It has since been identified in multiple, Greek–American and apparently unrelated Greek kindreds (Polymeropoulos *et al.*, 1997; Athanassiadou *et al.*, 1999; Markopoulou *et al.*, 1999; Papadimitriou *et al.*, 1999). The second mutation—a G-to-C transversion in exon 3 that, if translated, results in an Ala30Pro missense mutation—was identified in a German family (Krüger *et al.*, 1998). Several studies suggested that both mutations in the α-synuclein gene are rather rare causes of Parkinson's disease (Polymeropoulos *et al.*, 1996, 1997; Krüger *et al.*, 1998). However, the identification of these mutations in the α-synuclein gene provides evidence that α-synuclein is involved in the pathogenesis of Parkinson's disease. These efforts culminated in the identification of α-synuclein as a major component of Lewy bodies in sporadic Parkinson's disease and dementia with Lewy bodies (Spillantini *et al.*, 1997, 1998).

Recently, we reported results from reverse transcriptase–polymerase chain reaction (RT–PCR) restriction fragment length polymorphism (RFLP) experiments that showed low or absent expression of the G209A α-synuclein allele in a large Greek–American family (Family H) and suggested that haploinsufficiency may contribute to the pathogenesis in this form of ADFPD (Markopoulou *et al.*, 1999). Haploinsufficiency refers to a phenotype associated with inactivation of a single allele in a diploid organism (Cook *et al.*, 1998; Hu *et al.*, 1998). To determine whether haploinsufficiency underlies the pathogenesis of Parkinson's disease in other forms of ADFPD associated with different α-synuclein mutations, as well as in other families carrying the G209A mutation, we analysed the relationship between the expression levels of both the G88C and the G209A α-synuclein mutations and clinical phenotype in members of the German and additional Greek ADFPD families using quantitative mRNA and high performance liquid chromatography/mass spectrometry (HPLC/MS).

Material and methods

Patients

The German family investigated in this study is, to our knowledge, the only known pedigree carrying the Ala30Pro mutation in the α-synuclein gene, and has been described previously (Krüger *et al.*, 1998). Individual II-1 from the HEL-2 kindred has also been described previously (Chase *et al.*, 1999). In all three families, the parkinsonian phenotype is inherited as an autosomal dominant trait. The pedigrees are shown in Fig. 1 and the clinical characteristics of affected family members are summarized in Tables 1 and 2.

Cell lines

Human lymphoblastoid cell lines (EBV-transformed) were established, with informed consent, from three unrelated families with one or more individuals using a standard protocol (Neitzel, 1986). These cells were cultured in ISCOVE medium (Gibco, BRL, Rockville, MD, USA) with 10% fetal bovine serum (FBS) (Gibco), 8.5% $NaHCO_3$ L-glutamine (Gibco), 1% glutamine (Gibco) and 1% penicillin-streptamycin (PS) (Gibco). Cells were incubated at 37°C in a 5–6% CO_2 atmosphere.

Nucleic acid extraction and preparation of cDNA templates

Genomic DNA was prepared from lymphoblastoid cell lines using a QIAamp™ DNA Mini kit (QIAGEN, Hilden, Germany). RNA was isolated from freshly drawn blood using the PAXgene RNA isolation system (PreAnalytix, Valencia, CA, USA). Oligo(dT) primed cDNA was prepared from this RNA as described previously (Markopoulou *et al.*, 1999). RNA was isolated from lymphoblastoid cells using a RNeasy™ Mini Kit and a RNase-Free DNase Set (QIAGEN). Oligo(dT) primed cDNA was prepared from this RNA by reverse transcription using a RT kit (Takara, Shiga, Japan). The cDNA was used directly in TaqMan assays detecting the G88 and G88C alleles. In TaqMan assays detecting the G209 and G209A alleles, the cDNA obtained from reverse transcription alone was insufficient to perform TaqMan PCR. A PCR amplification was performed as described previously (Polymeropoulos *et al.*, 1997; Markopoulou *et al.*, 1999) using primers 1F and 13R, but using only ten cycles of amplification.

Expression of wild-type and mutant recombinant α-synuclein protein

For positive controls, we expressed wild-type and mutant α-synuclein recombinant protein using the IMPACT™-CN system (New England BioLabs, Beverly, MA, USA).

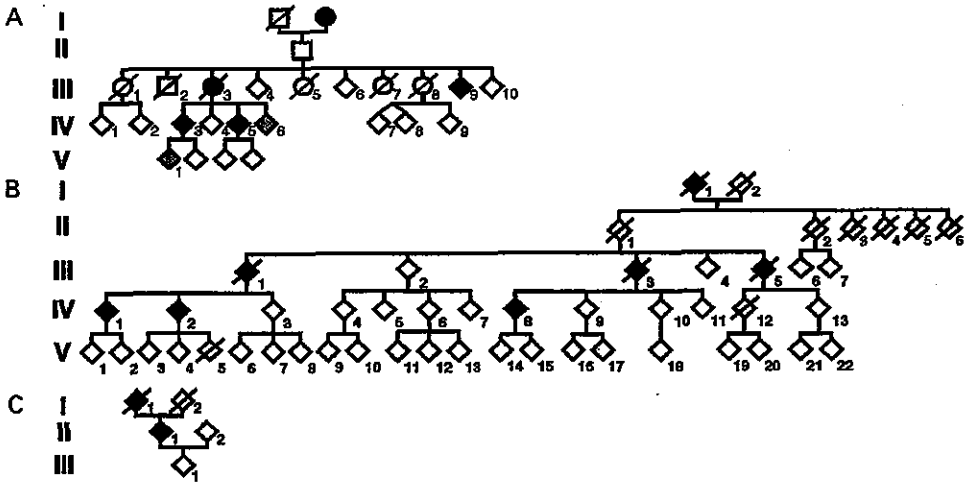

Fig. 1 Pedigree of the German and two Greek families. (**A**) Pedigree of the German family. (**B**) Pedigree of the Greek family HEL-1. (**C**) Pedigree of the Greek family HEL-2. The gender of the family members has been masked (diamonds) for reasons of confidentiality. Black boxes indicate affected heterozygotes and grey boxes unaffected heterozygotes.

Table 1 *The clinical characteristics of the German family*

	III-9	IV-3	IV-5	IV-6	V-1
Age (years)	76	65	58	52	33
Age at onset (years)	76	54	55	–	–
Disease duration (years)	<1	11	2	–	–
Initial symptom	Resting tremor	Rigidity	Rigidity	Bradydia-dochokinesia	Bradydia-dochokinesia
Bradykinesia	–	+++	+	(+)	(+)
Rigidity	+	+++	++	–	–
Resting tremor	+	–	–	–	–
L-dopa response	Nt	++	++	Nt	Nt

– = Not present; (+) = discrete/variable; + = mild; ++ = moderate; +++ = marked; Nt = No treatment

RT–PCR–RFLP and PCR–RFLP methods

RT–PCR on RNA isolated from fresh blood was performed as described previously using primers 1F and 13R (Polymeropoulos *et al.*, 1997; Markopoulou *et al.*, 1999). RT–PCR on RNA isolated from cell lines was performed using the TaKaRa RNA PCR kit (Takara). The conditions and primers for RT–PCR and PCR–RFLP were as described previously (Polymeropoulos *et al.*, 1997; Krüger *et al.*, 1998). PCR and RT–PCR products were digested with *Mva*I or *Tsp*45I and size-separated on 2%, 3% or 3.5% agarose gels.

Direct sequencing of RT–PCR products

We sequenced each RT–PCR product directly using a BigDye Terminator Cycle Sequencing Kit (Applied Biosystems, Foster City, CA, USA). Samples were then subjected to electrophoresis using an ABI PRISM 310 genetic analyser (Applied Biosystems).

Quantitative PCR using real-time TaqMan–PCR methods

Quantitative PCR was performed using the real-time TaqMan–PCR method, which has recently been established as a rapid and sensitive technique for the quantitation of gene expression. In this method, AmpliTaq DNA polymerase extends the primer and displaces the TaqMan probe through its 5′-to-3′ exonuclease activity (Heid *et al.*, 1996). The probes were labelled with a reporter fluorescent dye [6-carboxy-fluorescein dye (FAM)] at the 5′ end and a quencher fluorescent dye (TAMRA) at the 3′ end.

The expression level of the glyceraldehyde-3-phosphate dehydrogenase (GAPDH) gene was used as an endogenous control. Primers and a TaqMan probe for GAPDH (TaqMan GAPDH Control Reagent Kit) were purchased from Applied Biosystems. The probes for GAPDH were labelled with a reporter fluorescent dye [2,7-dimethoxy-4,5-dichloro-6-carboxy-fluorescein (JOE)] at the 5′ end.

Table 2 *The clinical characteristics of Greek families HEL-1 and HEL-2*

	IV-2	II-1
Age (years)	55	46
Age at onset (years)	42	39
Disease duration (years)	13	7
Initial symptom	Left arm rigidity/bradykinesia	Right arm rigidity
Bradykinesia	+++	+
Rigidity	+++	+
Resting tremor	–	–
Dementia	+	–
L-dopa response	Short-lived	+

– = Not present; + = mild; +++ = marked

Nuclease degradation of the hybridization probe removed the quenching effect of 6-carboxy-tetramethyl-rhodamine from the FAM or JOE fluorescent emission, thus increasing the peak fluorescent emission at 517 and 554 nm, respectively. No signal was emitted when the probe was intact.

Primers and TaqMan probes

Primers for PCR amplification and the TaqMan probe were designed on the basis of the published sequence of the α-synuclein mRNA. To selectively amplify the wild-type (G88, G209) and mutant (G88C and G209A) alleles, PCR reactions used different primers capable of amplifying these alleles selectively.

To amplify the wild-type G88 allele, primer set A (forward: 5′-AAGGACTTTCAAAGGCCAAGG-3′; reverse: 5′-CACCCTCTTTTGTCTTTCCTGC-3′) was used. To amplify the mutant G88C allele, primer set B (forward primer from primer set A; reverse: 5′-CACCCTCTTTTGTCTTTCCTGG-3′) was used. The TaqMan probe to detect these products had the sequence: 5′-AGTTGTGGCTGCTGCTGAGAAAACCAAACA-3′. To amplify the wild-type G209 allele primer set C (forward: 5′-GGTCTTCTCAGCCACTGTTAC -3′; reverse: 5′-TGGCAGAAGCAGCAGGAAA -3′) was used. To amplify the mutant G209A allele, primer set D (forward: 5′-TGGTCTTCTCAGCCACTGTTAT-3′; reverse primer from primer set C) was used. The TaqMan probe to detect these products had the sequence: 5′-CCTTGGTTTTGGAGCCTACATAGAGAACAC-3′.

The reaction mixture contained 25× TaqMan mixture (purchased from Applied Biosystems), the appropriate primer set, the TaqMan probe and the cDNA template in a total volume of 50 μl. The thermal cycling protocol consisted of 2 min at 95°C and 10 min at 95°C, followed by 45 cycles at 95°C for 15 s and 60°C for 1 min. TaqMan–PCR was analysed using a Model 7700 Sequence Detector (Applied Biosystems), which can measure fluorescence in real-time. The starting quantity of the target mRNA was calculated using the Sequence Detector software package version 1.6.3 (Applied Biosystems). The starting quantity of each target mRNA was normalized to that of the GAPDH endogenous control mRNA, allowing for measurement of the relative expression level of each RNA species.

For control TaqMan studies, we prepared constructs for both wild-type and mutant alleles in the plasmid vector pQBI25 (Takara). To obtain the wild-type α-synuclein gene, we performed RT–PCR using total RNA from normal brain tissue as a template. The RT–PCR product was subcloned into pQBI25. Site-directed mutagenesis of this clone was used to make constructs with the G88C and G209A mutations. We confirmed the specificity of the oligonucleotide primers for the wild-type and mutant alleles using three templates: the wild-type allele only; a mixture of wild-type and mutant alleles at a 1:1 ratio; and the mutant allele only.

Immunoprecipitation of α-synuclein from lymphoblastoid cells

Cells were washed three times with PBS and lysed on ice for 30 min by incubation in 1.0% NP40, 150 mM NaCl, 50 mM Tris–HCl pH 8.0. After centrifugation (20 000*g* for 30 min), immunoprecipitation was performed using an anti-α-synuclein antibody (BD Transduction Laboratories, Lexington, KY, USA) and the Seize™ X Protein G Immunoprecipitation Kit (PIERCE, Rockford, IL, USA).

One-dimensional sodium dodecyl sulphate–polyacrylmaide gel electrophoresis (SDS–PAGE)

Immunoprecipitated proteins were separated by SDS–PAGE on a 130 × 130 × 1 mm gel system (Nihon Eido Co., Tokyo, Japan) with separating (10% acrylamide) and stacking (3% acrylamide) gels containing 2.6% piperazine diacrylamide. Proteins in the gel were stained using Coomassie brilliant blue and protein profiles were determined using an image analyser, Master Scan from Scanalytics, Billerica, MA, USA.

In-gel digestion with trypsin and extraction of peptides

Bands containing α-synuclein protein were identified by comparison with expressed recombinant wild-type and

mutant α-synuclein proteins [molecular mass (Mr) 19000)]. The bands were excised and the proteins were digested with trypsin in the gel (Castellanos-Serra *et al.*, 1999).

Protein identification by HPLC/MS

Peptide mapping was carried out using an API QSTAR Pulsar hybrid mass spectrometer system consisting of a nano-electrospray and time-of-flight apparatus (Applied Biosystems). The QSTAR hybrid mass spectrometer was combined with a micro-liquid chromatograph (MAGIC 2002, Michrom Bioresources, Inc., Auburn, CA, USA) utilizing a 0.1 mm internal diameter × 50 mm $Magic_{C18}$ column. The solvent system consisted of (A) 0.1% formic acid, and (B) 0.1% formic acid/90% acetonitrile. The solvent programme was: 3% B for 2 min; a gradient of 1% B/min for 45 min; and 100% B for 5 min. The flow rate was 1 µl/min. Mass spectrometry conditions were: ion spray voltage, 3 kV; voltage for electron multiplier, 2400 V; and curtain gas nitrogen, 10 psi. Proteolytic fragments were identified using PROWL (ProFound, http://prowl.rockefeller.edu) and databases in the public domain (http://www.ncbi.nlm.nih.gov).

Results

Detection of α-synuclein mRNA expression in fresh blood

To address whether α-synuclein mRNA expression in lymphoblastoid cell lines is representative of, and relevant to α-synuclein mRNA expression in blood cells, we sought to verify that α-synuclein mRNA is expressed in lymphocytes. RT–PCR analyses were performed using total RNA templates isolated from freshly drawn blood. RNA was prepared using a method that preserves the integrity of RNA at the time of the blood draw, thus avoiding alterations in gene expression that can occur during storage of blood samples prior to RNA extraction. The results (Fig. 2) indicate that the expected 500 bp RT–PCR product is obtained in control fresh blood samples, the same size as the product obtained in lymphoblastoid cell lines established from control individuals and two affected G209A/+ heterozygotes (Fig. 2, lanes 1–7). No RT–PCR product was obtained in control reactions without RNA template or reverse transcriptase (Fig. 2, lanes 8–9). Direct sequencing of the RT–PCR products obtained using RNA templates from fresh blood confirmed that they are amplification products of α-synuclein mRNA (data not shown). These results demonstrate that α-synuclein mRNA is expressed in cells found in whole blood. Although these RT–PCR assays were not performed quantitatively, consistently greater RT–PCR product levels were seen in fresh blood RNA samples, suggesting that α-synuclein mRNA may be expressed at higher levels in lymphocytes than those in lymphoblastoid cell lines.

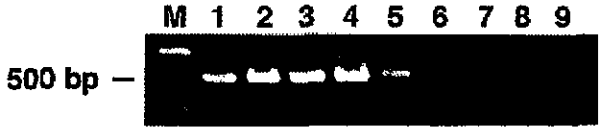

Fig. 2 α-Synuclein mRNA expressed in lymphocytes. The products of RT–PCR reactions using oligo-dT priming resolved on a 2% agarose gel are shown. Lane M: 100 bp ladder; lanes 1–3: reaction products using RNA template from replicate blood drawn from the same control individual; lances 4–5: reaction products using RNA template from either fresh blood (lane 4) or a lymphoblastoid cell line (lane 5) established from a second control individual; lanes 6–7: reaction products using RNA templates from lymphoblastoid cell lines established from two G209A/+ heterozygotes; lanes 8–9: reaction products were not seen in the absence of template (lane 8) or reverse transcriptase (lane 9). Sequence analysis of the 500 bp products (arrow) seen in lanes 1–4 confirms that they result from amplification of α-synuclein mRNA.

PCR and RT–PCR analysis with MvaI *and* Tsp*45I.*

Genomic DNA from individuals III-9, IV-3, IV-5, IV-6 and V-1 from the German family (Fig. 1A) was amplified by PCR using previously described primers (Krüger *et al.*, 1998). As previously reported, all five individuals possess the G88C mutation (Krüger *et al.*, 1998) (Fig. 3A). RFLP analysis of the RT–PCR products from these individuals indicated that individual IV-3, who is severely affected, did not exhibit the 379 bp RFLP fragment in *Mva*I digests of the RT–PCR products, indicating that the G88C allele is not transcribed. Individuals III-9, IV-5, IV-6 and V-1 exhibited the 379 bp RFLP RT–PCR fragment indicating that the G88C allele is transcribed (Fig. 3A). However, the exact amount of the G88C transcript could not be evaluated.

Genomic DNA from individuals IV-2 from the Greek family HEL-1 (Fig. 1B) and II-1 from the Greek family HEL-2 (Fig. 1C) was amplified by PCR using previously described primers (Polymeropoulos *et al.*, 1997). Both individuals possess the G209A mutation (Chase *et al.*, 1999). RFLP analysis of the RT–PCR products with *Tsp*45I (Polymeropoulos *et al.*, 1997) reveals that individual IV-2 (HEL-1), who is severely affected and has dementia, did not exhibit the 185 bp RFLP fragment indicating that the G209A allele is not transcribed, whereas individual II-1 (HEL-2) did exhibit the 185 bp fragment, indicating that the G209A allele is transcribed (Fig. 3B).

Direct sequencing of RT–PCR products

To confirm the above results, we performed direct sequencing of the RT–PCR products. Sequence analysis showed two nucleotides (G/C) at nucleotide position 88 of the coding region corresponding to the Ala30Pro substitution in two individuals (III-9 and IV-5). In contrast, the proband from IV-3, who had a severe phenotype, had only G in position 88. Similarly, in the Greek families, sequence analysis of

individual II-1 showed two nucleotides (G/A) at nucleotide position 209 corresponding to the Ala53Thr substitution, whereas sequence analysis of IV-2, who also has a severe phenotype, indicated only a G in position 209 (Fig. 3C and data not shown).

Quantitative PCR using real-time TaqMan-PCR method

Control study

We were able to discriminate between the wild-type and mutant alleles (Tables 3 and 4) using the protocol described above.

Expression of the mutant G88C and G209A allele

Expression analysis of the relative levels of mutant and wild-type alleles was performed using TaqMan real-time-PCR with mRNA as a template. We found different expression levels among affected members of the three families (Fig. 4). A summary of the clinical characteristics of the German family and the two Greek families is shown in Tables 1 and 2, respectively. The larger Greek kindred (HEL-1, Fig. 1B) has not been described previously, whereas the small kindred (HEL-2, Fig. 2C) has (Chase *et al.*, 1999). The two kindreds are not related genealogically.

In the German family, the expression of the mutant G88C allele was markedly reduced relative to the wild-type allele in individual IV-3. It is of interest that this individual presented with the most severe symptoms and longest duration of Parkinson's disease. In individual IV-5, who had mild symptoms with a disease duration of 2 years, the expression level of the mutant allele was about half that of the wild-type allele. In individual III-9, who had slight rigidity and resting tremor, the expression level of the mutant G88C allele was slightly lower than the wild-type allele. Both IV-6 and V-1 showed bradydiadochokinesis only, but did not fulfil the diagnostic criteria of Parkinson's disease (Calne *et al.*, 1992). Therefore, these members may be asymptomatic heterozygotes at present and may develop Parkinson's disease in the future. The expression of the wild-type allele in these two individuals was slightly reduced compared with the mutant allele. The TaqMan analysis could distinguish between the expression levels of the two alleles, even though it was difficult to distinguish individuals with a mild phenotype (III-9, IV-5) from carriers of the mutation (IV-6, V-1) by the RT–PCR RFLP method alone (Table 3, Figs 3 and 4).

Individual II-1 from the HEL-2 family developed parkinsonian symptoms that were responsiveto L-dopa at age 39 years. Seven years later, at age 46 years, this individual is able to function independently, requires no assistance with activities of daily living and, to date, has no cognitive impairment. The expression level of the mutant G209A allele was slightly higher than that of the wild-type allele. Individual IV-2 from the HEL-1 family developed parkinsonian symptoms at age 42 years, had a more rapid progression with diminishing response to L-dopa and has been unable to function independently, perform any activities of daily living without assistance and has had significant cognitive impairment for approximately the last 5 years. The expression of the mutant G209A allele was markedly reduced relative to that of the wild-type allele.

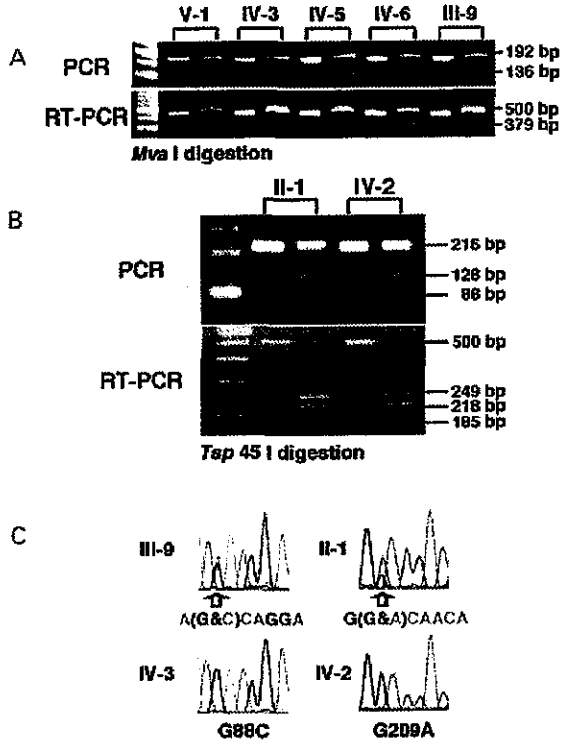

Fig. 3 PCR and RT–PCR analysis of affected members of the German and the two Greek families. Results of the PCR and RT–PCR analysis of the (**A**) German family members and (**B**) two Greek family members. In (**A**), both the PCR and RT–PCR products are digested with *MvaI*. For each individual, the left lane shows the undigested product and the right lane the digested product. The PCR products from individuals V-1, IV-3, IV-5, IV-6 and III-9 indicate that they are heterozygotes for the mutant allele (G88C) and the 192 bp, 136 bp and 56 bp fragments. In the RT–PCR products, individuals V-1, IV-6 and III-9 exhibited both the 500 bp (wild-type) and 379 bp (mutant) fragments, whereas individual IV-3 exhibited the 500 bp (wild-type) fragment only. In (**B**), both the PCR and RT–PCR products were digested with *Tsp*45I. For each individual, the left lane shows the undigested product and the right lane the digested product. The PCR products from individuals II-1 and IV-2 (heterozygotes for the G209A allele) exhibited the 216 bp, 128 bp and 88 bp fragments. In the RT–PCR products, individual II-1 exhibited the 500 bp, 249 bp, 218 bp and 185 bp fragments, whereas individual IV-2 exhibited the 500 bp, 249 bp and 218 bp fragments. (**C**) Sequence analysis of the RT–PCR products. Individual III-9 exhibits two peaks at position 88 (G/C) and individual IV-3 one peak (G) only. Individual II-1 exhibits two peaks (G/A) in position 209, whereas individual II-1 exhibits one peak (G) only.

Table 3 *Expression level of α-synuclein, G88C*

Control study			
Template	Primer A	Primer B	Primer A:Primer B
Wild-type	115.35 ± 10.43	0.22 ± 0.04	~1:0
Wild-type + mutant mixture	56.81 ± 6.61	64.94 ± 7.01	~1:1
Mutant	0.16 ± 0.07	118.14 ± 10.74	~0:1

Expression ratio of αsynuclein	III-9	IV-3	IV-5	IV-6	V-1
Wild-type	0.65 ± 0.13	1.12 ± 0.15	0.96 ± 0.17	0.45 ± 0.08	0.19 ± 0.03
Mutant	0.63 ± 0.04	0.26 ± 0.06	0.44 ± 0.37	0.60 ± 0.37	0.31 ± 0.01
Ratio (wild/mutant)	1.0	4.3	2.2	0.8	0.6

The upper table presents the results of control studies. Primer set A detects the normal allele. Primer set B detects the G88C allele. The lower table presents the expression data for each individual.

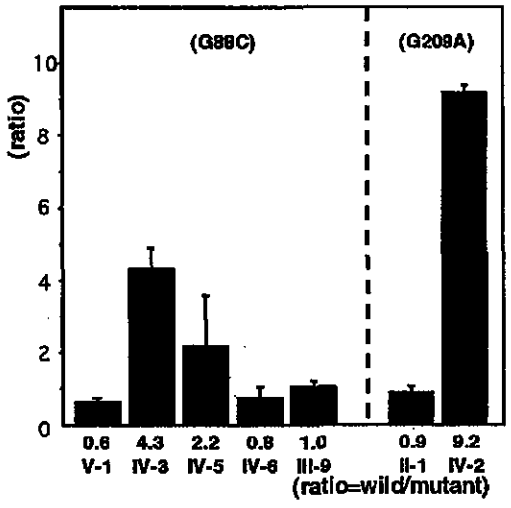

Fig. 4 Ratio of wild-type to mutant α-synuclein allele expression in lymphoblastoid cell lines. Vertical bars represent the ratio of wild-type to mutant allele expression. Individuals V-1, IV-3, IV-5, IV-6 and III-9 are members of the German family, individual II-1 is a member of Greek family HEL-2 and individual IV-2 is a member of Greek family HEL-1.

In summary, the results from all three families indicate that the ratio of expression of the wild-type to mutant α-synuclein alleles in lymphoblastoid cell lines correlates with the severity of symptoms of the affected individuals at the time of the cell line's establishment (Fig. 4, Tables 1, 2, 3 and 4).

Isolation of α-synuclein from lymphoblastoid cell lines

Coomassie brilliant blue stained SDS–PAGE gels identified protein bands of the size of Mr 19000 (Fig. 5), the same size as that of wild-type and mutant α-synuclein recombinant proteins.

Characterization of α-synuclein protein by HPLC/MS

Western blot analysis using the α-synuclein antibody detected α-synuclein in all the cell lines used in this study, including the normal lymphoblastoid cell lines (data not shown). Peptide mapping studies were undertaken to characterize the form(s) of the α-synuclein protein present in a subset of these lines. These results also indicate that α-synuclein is present in lymphoblastoid cells. Analysis of the HPLC fractions of trypsinized recombinant wild-type and mutant (Ala30Pro) α-synuclein protein demonstrated that the peaks $(M+2H)^{2+}$ at 415.7062 and 428.7469 corresponded to residues 24–32 of wild-type and mutant α-synuclein, respectively. HPLC/MS also identified the sequences of these peaks as QGVAEAAGK and QGVAEAPGK, respectively. Fragment ion data were collected on more than seven peptides from the lymphoblastoid cells established from individual IV-3. In total, these fragment ion masses matched 60% of the α-synuclein protein, confirming the presence of wild-type α-synuclein. In contrast, we could not find any peptides corresponding to mutant (Ala30Pro) α-synuclein in cell lines established from IV-3 (Fig. 6C and D). On the other hand, we could detect the peaks for peptides from both wild-type and mutant α-synucleins in the lymphoblastoid cells established from individual IV-6 (Fig. 6E and F). Only the peaks for peptides of the wild-type protein were detected in an unaffected, gene-negative member of this kindred (data not shown).

Discussion

We have used quantitative RT–PCR analysis to demonstrate that the mRNA expression of the mutant G88C and G209A alleles of the α-synuclein gene is significantly reduced relative to the wild-type allele in lymphoblastoid cell lines established from affected heterozygotes with a severe clinical phenotype. In contrast, these mutant alleles are expressed at levels similar to the wild-type allele in lymphoblastoid cell

Table 4 *Expression level of α-synuclein, G209A*

Control study			
Template	Primer C	Primer D	Primer C:Primer D
Wild-type	1076.44 ± 58.62	17.39 ± 0.89	~1:0
Wild-type + mutant mixture	522.33 ± 33.88	484.25 ± 23.59	~.1:1
Mutant	16.58 ± 0.91	968.98 ± 45.20	~.0:1

Expression ratio of α-synuclein	II-1	IV-2
Wild-type	3.82 ± 0.69	4.85 ± 0.32
Mutant	4.38 ± 0.35	0.53 ± 0.02
Ratio (wild/mutant)	0.9	9.2

The upper table presents the results of control studies. Primer set C detects the normal allele. Primer set D detects the G209A allele. The lower table presents the expression data for each individual.

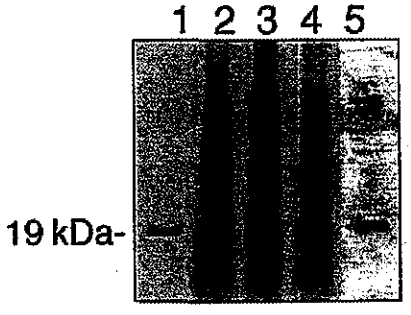

Fig. 5 Expression of α-synuclein protein. One-dimensional-SDS–PAGE of α-synuclein stained with CBB. Lane 1: positive control sample (recombinant wild-type protein); lane 2: IV-3; lane 3: IV-6; lane 4: normal human lymphoblastoid cell; lane 5: positive control sample [recombinant mutant (Ala30Pro) protein]. The position of the molecular weight marker is indicated on the left.

lines established from less severely affected heterozygotes or asymptomatic heterozygotes. HPLC/MS indicates that these allele-specific and disease-status specific alterations in mRNA expression are also reflected at the protein level. These results are consistent with the hypothesis that haploinsufficiency at the α-synuclein gene underlies the parkinsonian phenotype in kindreds with the G88C as well as the G209A mutation. To our knowledge, this is the first report in which (i) a quantitative analysis that determines the exact level of mRNA expression of both the wild-type and mutant alleles of α-synuclein and (ii) an analysis of the proteins encoded by the wild-type and mutant alleles has been used to support a hypothesis of haploinsufficiency in ADFPD.

While differences in the absolute levels of products obtained from individuals with the G88C and G209A mutations may reflect the different sites of the TaqMan probe and primers (which can influence the efficiency of amplification during RT–PCR) in control experiments involving mixtures of wild-type and mutant constructs, both wild-type and mutant templates could be detected (Tables 3 and 4). Thus, it is significant that we find that the ratios of wild-type to mutant transcripts differ between individual members of the families harbouring the G88C and G209A mutations. It is unlikely that these differences reflect clonal variation between populations of lymphoblastoid cells because they were confirmed in multiple experiments using independently generated cell lines. Rather, the data support the explanation that disease duration and severity may influence the expression of both the wild-type and mutant alleles. Disease progression and the presence of dementia appear to be associated with either increased expression of the wild-type allele or reduced expression of the mutant allele. This suggests that the ratio of expression levels of the wild-type to mutant α-synuclein alleles may be able to be developed as a clinical marker of this type of ADFPD, particularly since α-synuclein is normally expressed in lymphocytes.

We previously studied members of a large Greek–American kindred (Family H) and reported absent or significantly reduced levels of G209A allele expression in lymphoblastoid cell lines established from affected heterozygotes and some asymptomatic heterozygotes (Markopoulou *et al.*, 1999). Here, decreased levels of expression of the mutant allele at the α-synuclein gene are associated with the clinical phenotype in severely affected individuals only. One explanation for this involves methodological differences. We previously used RT–PCR RFLP only. There, the RT–PCR product is processed for RFLP analysis at the end-cycle point and the dynamics of PCR amplification make it difficult to interpret the magnitude of differences accurately. Indeed, in this study, it was difficult to distinguish individuals with a mild phenotype (III-9, IV-5) from carriers of the mutation (IV-6, V-1) by this method alone (Fig. 3). This issue is less of a concern as the TaqMan analysis used in this study allows for a real-time quantitative analysis.

What might be the consequences of differential and/or decreased expression of G88C and G209A mutant alleles? One might be that differential expression of the G88C and G209A alleles could result in different levels of the distinct

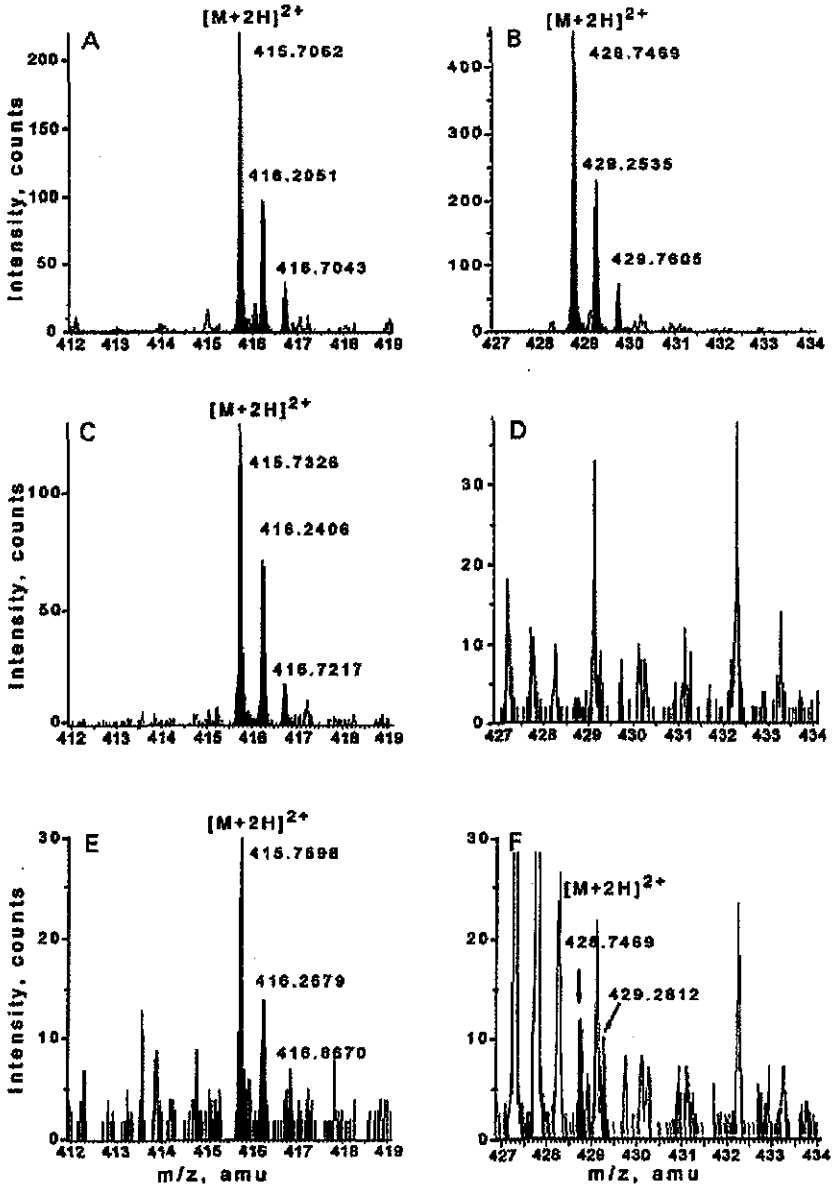

Fig. 6 Mass spectra for tryptic peptide of α-synuclein containing residues 24–32. These ion profiles show a representative fragment of α-synuclein detected within each sample. Selected peaks were identified by comparison with recombinant standards. (A) Standard (wild-type): QGVAEAAGK, Mr 829.5(retention time 4.22 min), (B) Standard (mutant Ala30Pro): QGVAEAPGK, Mr 855.5 (retention time 3.95 min), (C) IV-3 (wild-type). (D) IV-3 (mutant), (E) IV-6 (wild-type). (F) IV-6 (mutant).

Ala30Pro and Ala53Thr α-synuclein products produced by these alleles. Thus, differences between the functions provided by these mutant proteins and the wild-type proteins could underlie some aspects of the disease phenotype. Indeed, our HPLC/MS analysis revealed both wild-type and mutant proteins in a mildly affected G88C/+ individual, but only wild-type protein in a severely affected G88C/+ individual. That the mutant forms of α-synuclein are not functionally equivalent to wild-type α-synuclein has been suggested by multiple studies (e.g. Crowther *et al.*, 1998; Feany and Bender, 2000; Conway *et al.*, 2000*a*, *b*). However, it is difficult to extrapolate from these studies, which are based on *in vitro* over-expression or ectopic expression of mutant α-synuclein proteins, as to how reduced expression of a mutant form of α-synuclein would lead to neurodegeneration. An alternative explanation, which is also consistent with findings in other diseases exhibiting haploinsufficiency (Wilkie, 1994), is that the decreased expression of one allele leads to

a critical threshold level of α-synuclein that makes a cell more susceptible to being affected by the degenerative process. The sequestration of α-synuclein in Lewy bodies may contribute to a decrease in the amount of functional α-synuclein in the cell. Thus, compared with a cell having two wild-type alleles, a cell harbouring a mutant allele may be more susceptible to the consequences of sequestration of functional α-synuclein protein.

Phenotypes of complex diseases such as Parkinson's disease may be a manifestation of a complex molecular pathophysiology, and result from more than one contributing mechanism. For example, in myotonic dystrophy, two mechanisms—a trinucleotide repeat expansion causing haploinsufficiency of nearby genes and an abnormal protein kinase (myotonic dystrophy protein kinase) affecting RNA homeostasis (Korade-Mirnics *et al.*, 1998)—appear to be involved. The different phenotypic manifestations in familial parkinsonism may also reflect different molecular mechanisms. Thus, a reduction of α-synuclein gene expression may underlie the rapid rate of disease progression seen in this form of ADFPD as well as the presence of dementia, while a missense mutation (Ala30Pro and Ala53Thr) may underlie other aspects of the parkinsonian phenotype.

It is not clear whether the differences in the expression pattern of the α-synuclein alleles in lymphoblastoid cell lines reflect their expression patterns in the brain, and particularly in the substantia nigra. However, even though α-synuclein mRNA and protein isoform expression can be assessed in the brains of deceased individuals, the pattern will reflect the endpoint of the disease process and not the process that led to it. Our results suggest that as the neurodegenerative process unfolds, the expression of the mutant allele decreases and the expression of the wild-type allele increases to support the wild-type α-synuclein function in dopaminergic neurons. If there is a variation in the ratio of wild-type to mutant allele transcription among cells within the substantia nigra, cells that survive the neurodegenerative process may be those that are able to retain similar levels of wild-type and mutant allele transcription. In this event, one might not expect to see dramatic differences in the ratios between wild-type and mutant mRNA or protein expression in surviving cells. Nonetheless, further studies using brain tissue from affected patients to study mRNA and protein isoform levels, and to correlate these with disease severity are necessary to confirm our hypothesis of haploinsufficiency.

Acknowledgements

We wish to thank Drs Noriko Shindoh and Tsutomu Fujimura for valuable advice and Mei Wang for her generous gift of α-synuclein recombinant proteins. This study was supported in part by: a grant-in-aid for Scientific Research on Priority Areas from the Ministry of Education, Science, Sports, and Culture, Japan; a grant-in-aid for Health Science Promotion; a grant-in-aid for neurodegenerative disorders from the Ministry of Health and Welfare, Japan; a grant-in-aid from the UCR at the University of Nebraska-Omaha; a Centre of Excellence Grant from National Parkinson Foundation, Miami, Florida, USA; and an M. H. Udall NIH PD Centre of Excellence grant.

References

Athanassiadou A, Voutsinas G, Psiouri L, Leroy E, Polymeropoulos MH, Ilias A, et al. Genetic analysis of families with Parkinson's disease that carry the Ala53Thr mutation in the gene encoding alpha-synuclein. Am J Hum Genet 1999; 65: 555–8.

Calne DB, Snow BJ, Lee C. Criteria for diagnosing Parkinson's disease. [Review]. Ann Neurol 1992; 32 Suppl: S125–7.

Castellanos-Serra L, Proenza W, Huerta V, Moritz RL, Simpson RJ. Proteome analysis of polyacrylamide gel-separated proteins visualized by reversible negative staining using imidazole-zinc salts. Electrophoresis 1999; 20: 732–7.

Chase BA, Katechalidou L, Wszolek ZK, Markopoulou K. Early-onset, but not late-onset sporadic Parkinson's disease in the Greek population is associated with the G209A mutation at the α-synuclein gene [abstract]. Neurology 1999; 52 Suppl 2: A221–2.

Conway KA, Harper JD, Lansbury PT Jr. Fibrils formed in vitro from α-synuclein and two mutant forms linked to Parkinson's disease are typical amyloid. Biochemistry 2000a; 39: 2552–63.

Conway KA, Lee SJ, Rochet JC, Ding TT, Williamson RE, Lansbury PT Jr. Acceleration of oligomerization, not fibrillization, is a shared property of both α-synuclein mutations linked to early-onset Parkinson's disease: implications for pathogenesis and therapy. Proc Natl Acad Sci USA 2000b; 97: 571–6.

Cook DL, Gerber AN, Tapscott SJ. Modeling stochastic gene expression: implications for haploinsufficiency. Proc Natl Acad Sci USA 1998; 95: 15641–6.

Crowther RA, Jakes R, Spillantini MG, Goedert M. Synthetic filaments assembled from C-terminally truncated α-synuclein. FEBS Lett 1998; 436: 309–12.

Feany MB, Bender WW. A Drosophila model of Parkinson's disease. Nature 2000; 404: 394–8.

Gasser T, Muller-Myhsok B, Wszolek ZK, Oehlmann R, Calne DB, Bonifati V, et al. A susceptibility locus for Parkinson's disease maps to chromosome 2p13. Nature Genet 1998; 18: 262–5.

Heid CA, Stevens J, Livak KJ, Williams PM. Real time quantitative PCR. Genome Res 1996; 6: 986–94.

Hu G, Vastardis H, Bendall AJ, Wang Z, Logan M, Zhang H, et al. Haploinsufficiency of MSX1: a mechanism for selective tooth agenesis. Mol Cell Biol 1998; 18: 6044–51.

Kitada T, Asakawa S, Hattori N, Matsumine H, Yamamura Y, Minoshima S, et al. Mutations in the parkin gene cause autosomal recessive juvenile parkinsonism. Nature 1998; 392: 605–8.

Korade-Mirnics Z, Babitzke P, Hoffman E. Myotonic dystrophy: molecular windows on a complex etiology. [Review]. Nucleic Acids Res 1998; 26: 1363–8.

Krüger R, Kuhn W, Muller T, Woitalla D, Graeber M, Kosel S, et al.

Ala30Pro mutation in the gene encoding alpha-synuclein in Parkinson's disease. Nature Genet 1998; 18: 106–8.

Markopoulou K, Wszolek ZK, Pfeiffer RF, Chase BA. Reduced expression of the G209A α-synuclein allele in familial parkinsonism. Ann Neurol 1999; 46: 374–81.

Neitzel H. A routine method for the establishment of permanent growing lymphoblastoid cell lines. Hum Genet 1986; 73: 320–6.

Papadimitriou A, Veletza V, Hadjigeorgiou GM, Patrikiou A, Hirano M, Anastasopoulos I. Mutated α-synuclein in two Greek kindreds with familial Parkinson's disease: incomplete penetrance? Neurology 1999; 52: 651–4.

Polymeropoulos MH, Higgins JJ, Golbe LI, Johnson WG, Ide SE, Di Iorio G, et al. Mapping of a gene for Parkinson's disease to chromosome 4q21-q23. Science 1996; 274: 1197–9.

Polymeropoulos MH, Lavedan C, Leroy E, Ide SE, Dehejia A, Dutra A, et al. Mutation in the α-synuclein gene identified in families with Parkinson's disease. Science 1997; 276: 2045–7.

Spillantini MG, Schmidt ML, Lee VM, Trojanowski JQ, Jakes R, Goedert M. α-Synuclein in Lewy bodies. Nature 1997; 388: 839–40.

Spillantini MG, Crowther RA, Jakes R, Hasegawa M, Goedert M. α-Synuclein in filamentous inclusions of Lewy bodies from Parkinson's disease and dementia with Lewy bodies. Proc Natl Acad Sci USA 1998; 95: 6469–73.

Wilkie AO. The molecular basis of genetic dominance. [Review]. J Med Genet 1994; 31: 89–98.

Received June 1, 2002. Revised July 25, 2002.
Accepted July 29, 2002

Synthesis and Structure−Activity Relationships of an Orally Available and Long-Acting Analgesic Peptide, N^{α}-Amidino-Tyr-D-Arg-Phe-MeβAla-OH (ADAMB)

Tadashi Ogawa,[†] Tetsuhisa Miyamae,[†] Kimie Murayama,[‡] Kaori Okuyama,[§] Toru Okayama,[†,*] Masaki Hagiwara,[†] Shinobu Sakurada,[§] and Tadanori Morikawa[†]

Research Institute, Daiichi Fine Chemical Co. Ltd., 530 Chokeiji, Takaoka, Toyama 933-8511, Japan, Department of Biochemistry, Juntendo University School of Medicine, Tokyo 113-8421, Japan, and Department of Physiology and Anatomy, Tohoku Pharmaceutical University, 4-4-1 Komatsushima, Aoba-ku, Sendai 981-8558, Japan

Received July 30, 2001

A novel dermorphin tetrapeptide N^{α}-amidino-Tyr-D-Arg-Phe-MeβAla-OH (ADAMB) was designed based on the structures of several dermorphin tetrapeptide analogues, including N^{α}-amidino-Tyr-D-Arg-Phe-Gly-OH (ADA-DER), H-Tyr-D-Arg-Phe-βAla-OH (TAPA), and H-Tyr-D-Arg-Phe-Sar-OH (DAS-DER). These parent compounds were known to show a weak oral analgesic activity in animals and/or to possess a different mechanism of analgesia from other μ-opioid peptides. Six analogues of ADAMB were also synthesized to investigate the effect on potency of *N*-terminal amidination and *N*-methyl-β-alanine (MeβAla) substitution at position 4. Compounds were assessed using the tail pressure test in mice after subcutaneous and oral administration. Among the peptides tested, ADAMB showed the strongest oral antinociceptive activity, with an ED_{50} of 5.8 vs 22.2 mg/kg for morphine, as well as a 38-fold stronger activity after subcutaneous administration. ADAMB also showed long-lasting antinociceptive activity, with 50% of the maximum effect persisting in the tail pressure test at 10 h after oral administration (10 mg/kg). In contrast, orally administered morphine (80 mg/kg) showed a rapid decrease of activity in the same test and its antinociceptive effect disappeared within 4 h. When the antinociceptive effect of ADAMB was compared with that of analogues possessing βAla^4 (**1**) or Sar^4 (**2**), as well as analogues with *N*-substitution (**3**−**6**), it was found that both the N^{α}-amidino substitution and the MeβAla^4 were synergistically involved in creating ADAMB's exceptionally high antinociceptive activity.

Introduction

Since the isolation and identification of enkephalins[1] and other endogenous opioid peptides,[2] numerous peptidic analogues have been synthesized in attempts to develop an analgesic without the serious side effects of narcotics such as morphine.[3] However, these efforts have met with little success because of problems with side effects, low bioavailability, and high cost of production. Dermorphin (H-Tyr-D-Ala-Phe-Gly-Tyr-Pro-Ser-NH_2) was recently isolated from the skin of amphibians[4] and was reported to possess a potent and long-lasting opioid-like activity.[5] The *N*-terminal tetrapeptide of dermorphin is known to be the minimum sequence required for opioid activity,[6] although this fragment shows a lower potency than that of the parent heptapeptide.[7] Synthetic peptides derived from the dermorphin tetrapeptide, which have the sequence Tyr-D-AA^2-Phe-AA^4 (where AA^2 and AA^4 represent a certain amino acid), have been reported to show a potent agonist activity for the μ-opioid receptor.[8] Substitution of D-Ala at position 2 with D-Arg has been widely applied since the studies on D-Arg-kyotorphin were reported,[9] in order to increase the potency and the duration of action of the peptide. For example, Schiller[10] reported that DALDA (D-AA^2 = D-Arg, AA^4 = Lys-NH_2) is a potent and highly selective μ-opioid receptor agonist. Salvadori et al.[11] have extensively studied dermorphin analogues and have reported that N^{α}-amidination strengthens their antinociceptive activity. We recently found N^{α}-amidino-Tyr-D-Arg-Phe-Gly-OH (ADA-DER) as one of the most potent dermorphin tetrapeptides.[12] An analogue with *N*-methylation at position 4, H-Tyr-D-Arg-Phe-Sar-OH (DAS-DER),[13] shows selectivity for the μ_1-opioid receptor subtype and has oral antinociceptive activity in rats without inducing respiratory depression.[14] Sato et al.[15] recently reported that H-Tyr-D-Arg-Phe-βAla-OH (TAPA),[16] in which the amino acid residue at position 4 was substituted with β-alanine, had a more potent and longer-lasting antinociceptive effect than morphine after local or systemic administration and was a selective μ_1-opioid receptor agonist. In addition, the typical withdrawal symptoms that occurred upon cessation of administration or after treatment with naloxone, a classical μ-opioid antagonist, were less severe for TAPA than for morphine.[17] These observations encouraged us to explore the possibility of developing novel and orally active analgesic peptides without the adverse effects of morphine. On the basis of the structures of ADA-DER, DAS-DER, and TAPA, a compound featuring both N^{α}-amidination and *N*-methyl-β-alanine (MeβAla) at position 4 (ADAMB) was designed (Figure 1). This paper reports on the synthesis and the in vivo antinociceptive activity of ADAMB. To assess its potential as an oral analgesic, antinociceptive activity was evaluated in mice by the tail pressure test and was compared with

* To whom correspondence should be addressed. Tel: +81(766)21-3456. Fax: +81(766)26-4439. E-mail: okayama@daiichi-fcj.co.jp.
[†] Daiichi Fine Chemical Co. Ltd.
[‡] Juntendo University School of Medicine.
[§] Tohoku Pharmaceutical University.

10.1021/jm010357t CCC: $22.00
Published on Web 10/08/2002

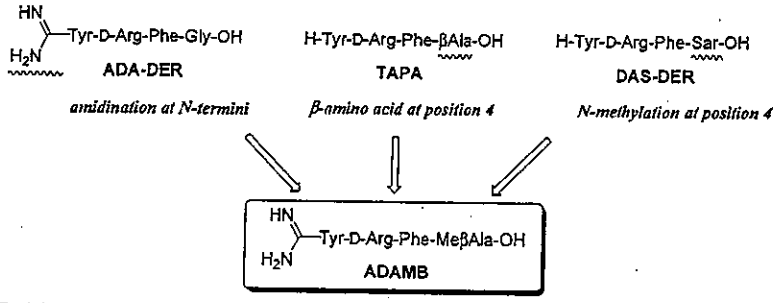

Figure 1. Design of ADAMB based on the structure of several dermorphin tetrapeptide analogues.

Scheme 1[a]

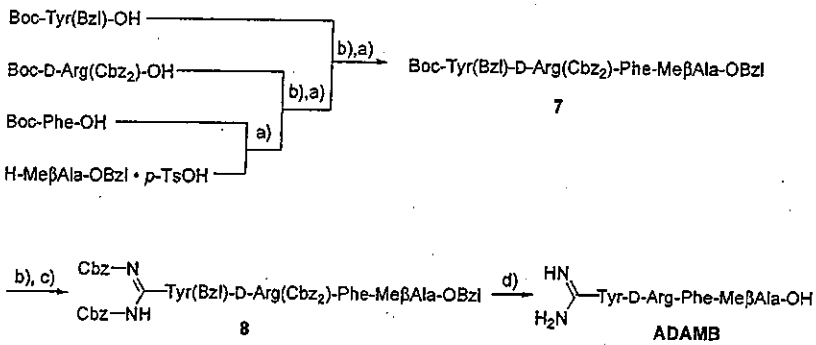

[a] Reagents: (a) WSCI–HOBt. (b) 4 N HCl in EtOAc. (c) 1-(Bis-benzyloxycarbonylguanyl)pyrazole, Et_3N in DMF. (d) H_2/Pd–C in AcOH.

that of morphine. In addition, six analogues of ADAMB were synthesized to clarify the influence of *N*-amidination and MeβAla[4] substitution on antinociceptive activity and the data obtained regarding the structure–activity relationships (SARs) are also discussed here.

Chemistry

ADAMB was successfully synthesized by both solid phase and solution phase methods. The N^{α}-Fmoc strategy was used for solid phase synthesis, employing a *p*-alkoxybenzyl alcohol resin (Wang resin).[18] N^{α}-Fmoc-protected amino acids were added sequentially, using 2-(1*H*-benzotriazol-1-yl)-1,1,3,3-tetramethyluronium hexafluorophosphate (HBTU) with 1-hydroxybenzotriazole (HOBt) as the coupling reagents in 1-methyl-2-piperidone (NMP). *N*-Terminal amidination was performed on the resin after assembly of the peptide chain by removal of the Fmoc group followed by treatment with a mixture of 1*H*-pyrazole-1-carboxamidine hydrochloride[19] and diisopropylethylamine in dimethylformamide (DMF). Analogues bearing βAla (**1**) or Sar (**2**) at position 4 were also synthesized using the same method. To investigate the effect of *N*-terminal substitution on antinociceptive activity, four other analogues of ADAMB were also synthesized by the solid phase method. These analogues had structures that could be represented by the general formula of R-Xaa-D-Arg-Phe-MeβAla-OH, where R and Xaa are the *N*-terminal substituent and the amino acid residue, respectively. They were designated as compounds **3** (R = H, Xaa = Tyr), **4** [R = H, Xaa = *N*-methyltyrosine (MeTyr)], **5** [R = none, Xaa = *N,N*-dimethyltyrosine (Me_2Tyr)], and **6** (R = acetyl, Xaa = Tyr, βAla[4] instead of MeβAla[4]). To obtain a substantial amount of the compound for animal tests, ADAMB was subsequently synthesized by a solution method using 1-ethyl-3-(3-dimethylaminopropyl)carbodiimide hydrochloride (WSCI·HCl) with HOBt as the coupling reagent (Scheme 1). The side chain functional groups and the C-terminal carboxylic acid were fully protected by Cbz or Bzl protection groups, which were simultaneously removed by catalytic hydrogenolysis in the presence of Pd on charcoal. Thus, starting with H-MeβAla-OBzl, N^{α}-Boc-protected amino acids were coupled sequentially to give the fully protected tetrapeptide (**7**). An N^{α}-amidino group was introduced in a bis-Cbz-protected form using (benzyloxycarbonylimino-pyrazol-1-yl-methyl)carbamic acid benzyl ester.[20] Then, all of the protecting groups were cleanly removed by catalytic hydrogenation to give the desired product (ADAMB) with a high purity. This method is used to facilitate the large-scale synthesis of compounds containing the highly polar and hydrophilic functional groups. All final products were purified by reverse phase C18 flush column chromatography with elution using aqueous CH_3CN containing 0.1% acetic acid to afford the purified products (>95% purity by high-performance liquid chromatography (HPLC) analysis in two diverse systems). The structure of the final product was confirmed by ^{1}H NMR and by high-resolution mass spectral (HRMS) analysis.

Biological Results

The synthesized compounds were tested to determine their relative opioid receptor binding affinity by displacement of selective radioligands from mice spinal cord or guinea pig brain membrane preparations. [^{3}H][D-Ala^2,MePhe^4,Gly-ol^5]enkephalin ([^{3}H]DAMGO), [^{3}H]deltorphin-II, and [^{3}H]U-69593 were used for determining the μ-, δ-, and κ-affinity, respectively. The results of these binding assays are summarized in Table 1. ADAMB showed a high binding affinity for the μ-opioid receptor, which was comparable to that of DAMGO in the [^{3}H]DAMGO binding assay. When com-

Table 1. Receptor Binding Assay of ADAMB and Its Analogues

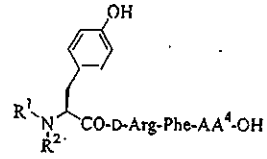

				[^{3}H]DAMGO (μ)		[^{3}H]deltolphin-II (δ)	[^{3}H]U-69593 (κ)
compd	R^1	R^2	AA^4	IC_{50}[a] (nM)	relative potency[b]	IC_{50} (nM)	IC_{50} (nM)
ADAMB	$H_2NC(=NH)-$	H–	MeβAla	12.9 ± 3.4	0.90	>1000	>1000
1	$H_2NC(=NH)-$	H–	βAla	20.8 ± 3.2	0.56	>1000	>1000
2	$H_2NC(=NH)-$	H–	Sar	32.9 ± 12	0.35	>1000	>1000
3	H–	H–	MeβAla	10.2 ± 4.2	1.14	>1000	>1000
4	CH_3-	H–	MeβAla	45.0 ± 11	0.26	>1000	>1000
5	CH_3-	CH_3-	MeβAla	101 ± 20	0.11	>1000	>1000
6	CH_3CO-	H–	βAla	>1000	<0.01	>1000	>1000
DAMGO				11.6 ± 1.7 (5.07 ± 0.68)[c]	1.00	>1000	>1000
deltorphin-II				nd		13.7 ± 2.3[c]	nd
U-69593				nd		nd	3.17 ± 0.35[c]

[a] Concentration that gives half-maximal effect. Data are given as the mean ± SEM (n = 3). [b] Relative potencies are on a molar basis (DAMGO = 1). [c] K_i value.

Table 2. In Vivo Antinociceptive Activity of ADAMB and Its Analogues (Tail Pressure Test)

	MPE %max[a]		ED_{50} (mg/kg)[b]		
compd	sc (1 mg/kg)	po (10 mg/kg)	sc	po	sc/po (%)
ADAMB	100 ± 0.0	82 ± 6.4	0.089 (0.06–0.15)	5.8 (3.6–9.4)	1.5
1	93 ± 6.9	18 ± 4.8	0.32 (0.22–0.46)	19 (9.3–37)	1.7
2	90 ± 5.0	26 ± 11	0.39 (0.25–0.61)	18 (11–29)	2.2
3	91 ± 5.1	31 ± 8.8	0.39 (0.22–0.69)	nd	
4	87 ± 9.7	34 ± 9.7	0.21 (0.13–0.34)	15 (9.0–25)	1.5
5	29 ± 11	13 ± 5.5	nd	nd	
6	<10	<10	nd	nd	
morphine	nd	nd	3.3 (2.2–4.9)	22 (14–36)	15

[a] Data were taken at 1.5 h after drug administration and are given as the mean ± SEM for groups of 10 mice. [b] The ED_{50} value was estimated at the time of peak activity and are given as the mean value with its 95% confidence limit for 10 mice.

pared to a compound without *N*-terminal amidination (**3**), ADAMB had almost the same binding affinity, whereas *N*-terminal methylation (**4**) or dimethylation (**5**) caused a significant decrease of affinity for the μ-opioid receptor. On the other hand, modifications at position 4 caused a decrease of μ-affinity. Thus, each of the analogues in which MeβAla^4 was substituted by βAla^4 (**1**) or Sar^4 (**2**) showed a decline of μ-affinity to one-half or one-third of that for ADAMB, respectively. An analogue with *N*-terminal acetylation (**6**) did not show any strong affinity (IC_{50} > 1000 nM) for the μ-opioid receptor. None of the compounds showed any significant affinity (IC_{50} > 1000 nM) for either the δ- or the κ-opioid receptor, which indicated that these analogues show specific affinity for the μ-opioid receptor relative to the δ- and the κ-opioid receptors.

The compounds were tested to assess their in vivo antinociceptive potency (Table 2) using the tail pressure test[21] after subcutaneous (sc) and oral (po) administration to mice. The maximum possible effect (MPE %) was initially measured at fixed doses of 1 subcutaneously and 10 mg/kg orally, after which analogues with a high potency were assessed for antinociceptive activity on the basis of ED_{50} values. ADAMB showed a very strong antinociceptive activity in mice after sc administration, and its ED_{50} value was 37 times higher than that of morphine. ADAMB was significantly antagonized by sc pretreatment with naloxone (data not shown) in the same mouse test. As expected from the design of ADAMB, its po antinociceptive activity was also strong and the ED_{50} value was 3.8 times higher than that of morphine. To assess bioavailability, the ED_{50} dose ratio (sc/po) of ADAMB was calculated and compared with that of morphine. The ratio for ADAMB was 1.5%, while that for morphine was 15%. Substitution of MeβAla at position 4 with either βAla (**1**) or Sar (**2**) (corresponding to TAPA and DAS-DER with N^{α}-amidination) caused a significant decrease in potency to one-third of that for ADAMB after both sc and po administration. However, both compound **1** and compound **2** still had a stronger sc antinociceptive activity than morphine and comparable po activity. The compound without *N*-terminal substitution (**3**) also showed a significant decrease of antinociceptive activity when compared with ADAMB. *N*-Terminal monomethylation (**4**) did not affect the antinociceptive activity when compared to the analogue with an *N*-terminal primary amine (**3**), whereas substitution of both hydrogens at the amino terminal with methyl groups (**5**) caused a substantial decrease of activity. Comparison of the ED_{50} ratio (sc/po) for ADAMB with those of compounds **1**, **2**, and **4** showed that the bioavailability was unchanged by modification at the *N*-terminal and position 4. To further investigate the role of the amino terminal, an analogue bearing an *N*-acetyl group (**6**) was synthesized. This modification canceled the basicity and nucleophilicity of the amino group and resulted in no measurable antinociceptive

Table 3. In Vivo Antinociceptive Activity of ADAMB and Selected Analogues (Hot Plate Test)

compd	ED_{50} (sc, mg/kg)[a]	compd	ED_{50} (sc, mg/kg)[a]
ADAMB	0.07 (0.02–0.24)	3	0.15 (0.08–0.21)
1	0.21 (0.12–0.36)	4	0.11 (0.05–0.24)
2	0.08 (0.3–0.21)	morphine	1.7 (0.7–3.8)

[a] The ED_{50} value was estimated at the time of peak activity and was given as the mean value with its 95% confidence limit for 10 mice.

effect, even though the *N*-acetamino group was virtually the same size and shape as the *N*-terminal guanidino group.

ADAMB and several analogues (**1**–**4**), which showed strong antinociceptive activity in the mouse tail pressure test, were assessed for their antinociceptive potency in a mouse hot plate test after sc administration (Table 3). Like the tail pressure test, ADAMB showed the strongest antinociceptive activity among the compounds tested. Morphine was 24 times less potent in terms of the ED_{50} value than ADAMB. The Sar[4] analogue **2** showed a comparable ED_{50} value to that of ADAMB, but **2** was significantly less active than ADAMB in the tail pressure test. With the exception of compound **2**, which is an α-amino acid analogue showing a difference at position 4, the antinociceptive results obtained in the hot plate test showed a good correlation with the data from the tail pressure test.

Figure 2 shows the time course of the antinociceptive effect of sc administered morphine and ADAMB in the mouse tail pressure test. ADAMB (Figure 2B) produced dose-related stronger antinociceptive activity than morphine (Figure 2A). The total duration of action for ADAMB was over 10 h at a maximally active dose of 0.2 mg/kg, whereas the activity of morphine disappeared within 4 h at a dose of 10 mg/kg.

As shown in Figure 3B, oral ADAMB also had dose-related and significant antinociceptive activity, with 50% of MPE being maintained at 10 h after administration at the maximally active dose of 10 mg/kg. The peak effect appeared 4–6 h after administration at this dose. Morphine showed its maximum antinociceptive activity at a dose of 80 mg/kg with a peak at 60 min after administration. Oral ADAMB had a far longer duration of action than morphine, which was effective for less than 4 h after administration (Figure 3A).

To clarify the role of the μ-opioid receptor subtypes, μ_1 and μ_2, in the antinociceptive effect of ADAMB on noxious stimuli, pretreatment (sc) with a μ_1 selective opioid receptor antagonist, naloxonazine, or a nonselective antagonist, naloxone, was done in the mouse tail pressure test (Figure 4). Then, the results were compared with those for morphine (Figure 5). Either naloxonazine (35 mg/kg) or naloxone (0.2 mg/kg) pretreatment at 24 h before administration of ADAMB (0.5 mg/kg) markedly attenuated its antinocieptive action, and the difference in the extent of attenuation was not significant. In contrast, pretreatment with naloxonazine showed only partial attenuation of the antinociceptive effect of morphine (10 mg/kg), while naloxone completely suppressed it.

Discussion

Since the isolation of dermorphin, many analogues have been synthesized and extensively investigated in attempt to develop new peptide analgesics as well as to determine their pharmacological properties.[22] Among them, TAPA and DAS-DER, in which the C-terminal amino acid residue at position 4 is substituted with β-Ala or Sar, respectively, are known to have an antinociceptive activity even after oral administration. Therefore, we expected that a tetrapeptide bearing MeβAla at position 4 could show increased oral antinociceptive activity by combining homologation and *N*-methylation. We have recently synthesized more than 50 compounds with the general structure of N^{α}-amidino-Tyr-D-Arg-Phe-X (where X represents various amino acids, amides, amino esters, and amino alcohols) and have found that they show strong antinociceptive activity comparable to that of morphine after oral administration.[12] Therefore, a combination of these modifications seemed likely to amplify oral activity and to be a promising approach for the development of an orally active analgesic peptide. To confirm our hypothesis, we performed an in vivo test using mice for initial evaluation of the compounds synthesized. As expected, ADAMB showed very potent oral antinociceptive activity and was approximately 4 times as strong as morphine. In our preliminary experiment using a similar mouse test that we employed in this study, the antinociceptive effect of ADAMB was five times stronger than that of TAPA after sc administration and seven times stronger after po administration (based on ED_{50} values). However, the bioavailability of ADAMB may not be sufficient for an oral analgesic since its dose ratio (sc/po) was 10-fold smaller than that of morphine (based on ED_{50} values). Comparison of ADAMB with analogue **3** (no N^{α}-substitution) showed that N^{α}-amidination markedly improved the antinociceptive effect after both sc and po administration, while the dose ratio (sc/po) of the ED_{50} values did not change as compared with that of analogue **4**. This indicated that *N*-amidination is important for antinociceptive activity but not for bioavailability. Likewise, the combination of *N*-methylation and homologation of the amino acid residue at position 4 did not achieve any increase in bioavailability, although significant improvement of antinociceptive activity was observed (ADAMB vs compounds **1** and **2**). Therefore, further structural modification of ADAMB, including alteration of other parts of the molecule, will be necessary before this type of compound can be used as an oral analgesic.

The presence of an *N*-terminal amino group in opioid peptides is crucial for a strong agonist effect on the opioid receptors.[23] *N*-Terminal amidination of dermorphin tetrapeptides is known to decrease the in vitro affinity for opioid receptors, while it strengthens the in vivo antinociceptive acitvity.[24] However, little is known about the SARs of *N*-terminal amidination as well as the effect of this modification on other opioid peptides. In the present study, the antinociceptive activity of the *N*,*N*-dimethylated analogue (**5**) showed a considerable decrease, whereas the monomethylated analogue (**4**) retained similar activity to that of the unsubstituted analogue (**3**). On the other hand, *N*-acetylation led to a decrease of activity. These observations suggest the importance of an *N*-terminal amino group that retains basicity and, unlike most of the nonpeptide μ-agonists

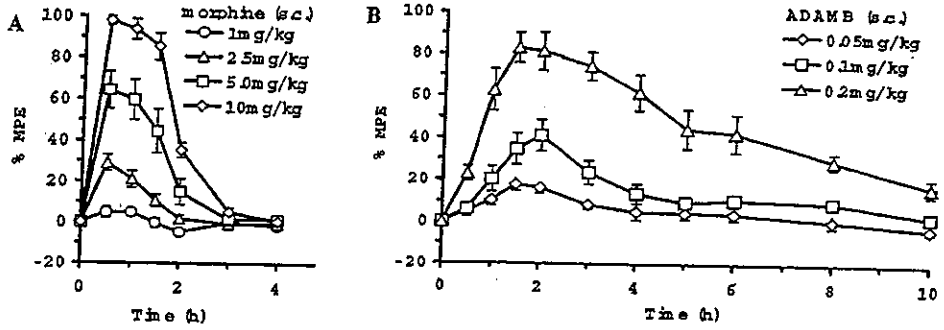

Figure 2. Time course of the antinociceptive effect of subcutaneous morphine (A) and ADAMB (B) in the mouse tail pressure test. The doses used are shown in the figure. Data are given as the mean ± SEM for groups of 10 mice.

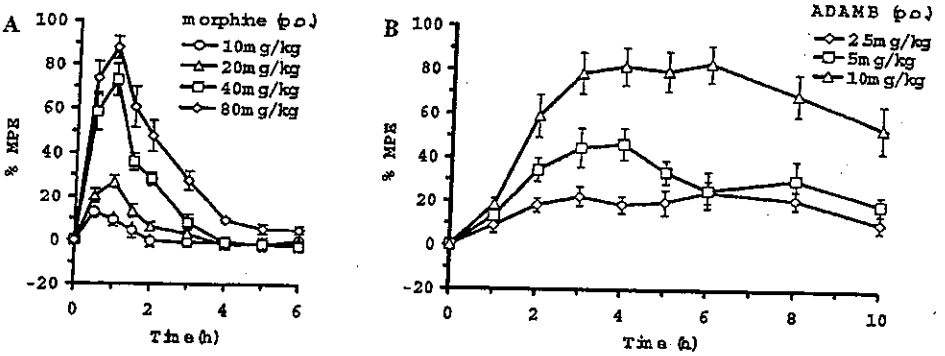

Figure 3. Time course of the antinociceptive effect of oral morphine (A) and ADAMB (B) in the mouse tail pressure test. The doses used are shown in the figure. Data are given as the mean ± SEM for groups of 10 mice.

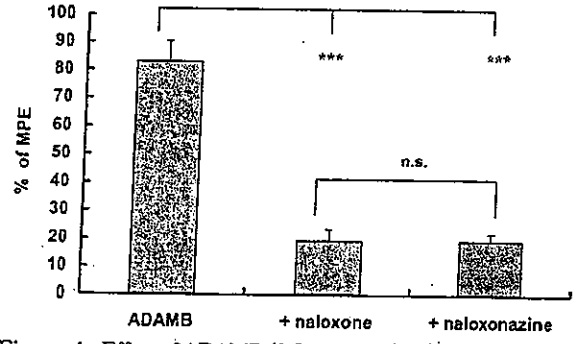

Figure 4. Effect of ADAMB (0.5 mg/kg, sc) after pretreatment with naloxone or naloxonazine in the mouse tail pressure test. Naloxone (0.2 mg/kg, sc) was given 5 min before ADAMB. Naloxonazine (35 mg/kg, sc) was given 24 h before ADAMB. Data are the mean ± SE for 10 mice. *** < 0.001 vs ADAMB alone (Tukey's test).

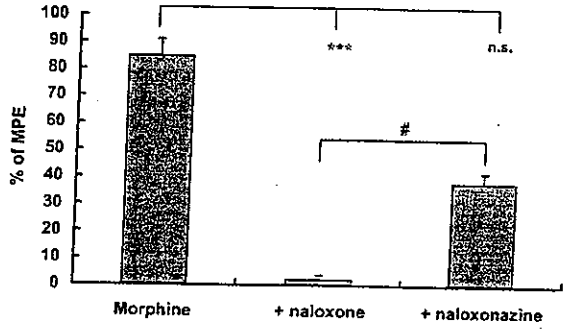

Figure 5. Effect of morphine (10 mg/kg, sc) after pretreatment with naloxone or naloxonazine in the mouse tail pressure test. Naloxone (0.2 mg/kg, sc) was given 5 min before morphine. Naloxonazine (35 mg/kg, sc) was given 24 h before morphine. Data are the mean ± SE for 10 mice. *** < 0.001 vs morphine alone; # < 0.05 for pretreatment with naloxone vs pretreatment with naloxonazine (Tukey's test).

that commonly possess a tertiary amine, at least one unsubstituted amine hydrogen in Tyr[1] as well.

ADAMB has an exceptionally long-lasting antinociceptive activity after both sc and po administration as does TAPA.[15] Comparison of the time−course of the antinociceptive effect of ADAMB with that of morphine showed that the onset was slower for ADAMB after either sc or po administration. The peak time of analgesia after administration was accordingly shifted to later than that for morphine, being 1.5−2 (sc) and 3−4 h (po) for ADAMB vs 0.5 (sc) and 1 h (po) for morphine, respectively. The reason for the stronger and longer antinociceptive activity of ADAMB along with its slow onset is still unclear, although we assume that it is partly due to enhancement of the compound's stability. It could be also explained by the slow and continuous influx of ADAMB into the central nervous system across the blood−brain barrier (BBB) in addition to tight binding of the peptide with the μ-opioid receptors. These properties would be related to a low clearance rate from the blood as well as the peptide's extremely high stability to enzymatic hydrolysis. Nevertheless, this feature may be advantageous in combination with the higher efficacy of the compound relative to morphine. even though slow release morphine formulations such as 12 h oral preparations[3] have been widely accepted for clinical use. The high efficacy and long duration of